Statistics of turbulence subgrid-scale stresses: Necessary conditions and experimental tests

Charles Meneveau
Department of Mechanical Engineering, The Johns Hopkins University, Baltimore, Maryland 21218

(Received 9 March 1993; accepted 7 July 1993)

Some thoughts are presented regarding the question: when can a subgrid-scale model yield correct statistics of resolved fields in a large-eddy simulation (LES) of turbulent flow. The filtered Navier–Stokes equations are used to find *necessary* conditions on the statistical properties of the modeled subgrid-scale stress tensor, for statistical equivalence between a "real" and a modeled (*via* LES) turbulent velocity field. When trying to formulate *sufficient* conditions, an unclosed hierarchy of expressions is obtained, essentially due to the "turbulence problem" of the resolved scales of motion. Experimental (*statistical a priori*) testing of subgrid-scale models is performed, based on single-probe measurements in grid turbulence and on several key assumptions. Three versions of the eddy-viscosity model are considered: constant eddy viscosity, subgrid kinetic energy, and the usual Smagorinsky eddy viscosity. Measured joint moments between filtered velocity and real or modeled subgrid scale stresses show that both energy and enstrophy dissipation can be properly captured, with a single value of the model constants over a significant range of filter widths. These results are used to examine a new subgrid model based on enstrophy equilibrium. The cross-correlation function of filtered velocity with the subgrid stress tensor is measured, which is of special importance for large-scale energy spectra. No significant differences are observed between the different models, and it is found that they predict trends in the stress-velocity cross-correlation quite well. The results show that, in nearly isotropic turbulence, the eddy-viscosity subgrid models correctly reproduce statistical trends necessary for the accurate LES prediction of energy spectra and enstrophy evolution.

I. INTRODUCTION

Large-eddy-simulation (LES) is rapidly growing in importance as a technique for the calculation of turbulent flows in simple and complex geometries (Reynolds, 1990;[1] and Rogallo and Moin, 1984[2]). The discarded scales of motion act on the resolved velocity field as new stresses, which need to be modeled (subgrid scale, or SGS, modeling). The fact that the modeling is done at a length scale smaller than the flow integral scale raises the hope that the models can be more "universal" (flow independent) than their counterparts for Reynolds stresses. Nevertheless, there is a striking difference between SGS and Reynolds stresses modeling. Whereas for the latter there exists a large amount of information, e.g., measured Reynolds stress profiles in a variety of flows, little is known about the subgrid-scale stresses. The purpose of this paper is to examine through some elementary considerations what information about subgrid stresses is needed, and to obtain such information for a simple turbulent flow.

To inquire about the correctness of a particular SGS model one can perform the simulation using the model and compare the results with experimental data. For instance, one can compare measured mean velocity profiles (for which there is a lot of experimental and direct numerical simulation (DNS) data available) with those resulting from the LES. This approach is called *a posteriori* model testing. It has been used to show that LES using simple models, such as the Smagorinsky eddy viscosity, can yield good predictions, both in terms of mean velocity profiles, second-order moments and even energy spectra. This is true quite generally for free shear flows, although the model constants need some adjustments from flow to flow. The recent "dynamic model"[3,4] has so far yielded very encouraging results.[5,6] Higher-order statistics were considered recently in Ref. 7 for isotropic turbulence, and good LES predictions were obtained. It has even been argued that if no SGS model is used, and one relies entirely on numerical ("flux corrected") diffusion, reasonable results can be obtained under certain circumstances.[8] On the other hand, SGS modeling for nonequilibrium flows, for the near-wall behavior, etc., still presents considerable challenges. In this context, a drawback of *a posteriori* testing is that it is not always easy to pinpoint the physics that cause a model to work (or not to work), and to separate the SGS model from other elements that affect the results, such as numerics.

Another approach, called *a priori* testing, consists of the direct use of known, fully resolved, velocity fields. They are filtered to compute the stresses, and these can then be compared on a local and instantaneous basis with features of the large-scale field, which are also known. In this fashion, a direct test can be made about the physical content of a model, without actually performing the LES. This approach has so far been employed using direct numerical simulations; see e.g., Clark *et al.* (1979),[9] McMillan and Ferziger (1979),[10] Piomelli (1988),[11] Meneveau *et al.* (1992),[12] Lund and Novikov (1992),[13] Domaradzki *et al.* (1993),[14] Härtel and Kleiser (1993),[15] etc. For recent work, where both *a priori* and *a posteriori* testing is employed, see Horiuti (1993).[16] In general, the results of *a priori* testing based on DNS data have been discouraging:

 1070-6631/94/6(2)/815/19/$6.00

At a local instantaneous level, the real and modeled stresses are almost never the same, exhibiting very low correlation coefficients. This observation is made, even when very sophisticated regression techniques are employed.[12] However, it has been remarked quite often (e.g., Reynolds, 1990[1]) that the low correlation between stresses and predictions does not necessarily translate into poor results when a model is actually implemented in a LES. In other words, the *a priori* analysis gives an excessively pessimistic view of the modeling. From these considerations it becomes clear that, despite its own shortcomings, *a posteriori* testing is to remain of central importance in the study of model performance, and in no way can be replaced by *a priori* tests. Although in the present work the focus is on a statistical version of the latter, we stress that the two approaches are to be viewed as complementing each other.

Having reviewed these basic aspects and difficulties in the study of SGS parametrization, we now consider placing conditions on the model that are weaker than those usually expected in *a priori* testing. During a LES, the dynamics of the small scales is not captured. Thus it is clear that an exact, deterministic relation between stresses and functionals of the resolved field must be impossible to formulate. Also (except for control purposes or for short-term predictability[17]) one is not necessarily interested in a particular realization of the LES since the hydrodynamic evolution of the large scales is typically expected to be chaotic anyway, even with a "perfect" subgrid closure. Such considerations suggest placing weaker conditions on the stresses: namely, that they cause the LES to reproduce correct *statistical* features of the flow field. The question then becomes, what conditions must they satisfy to correctly generate some desired statistical feature of the flow? This question, as well as how such conditions can be used in *statistical a priori* testing of models using experimental data, are the main themes of this paper.

To allow for a more focused discussion, an incompressible turbulent flow obeying the Navier–Stokes equations in a domain Ω, bounded by $\partial\Omega$, is considered. It follows that $\tilde{u}_i(\mathbf{x},t)$, the convolution of the real velocity field with some spatial filter of characteristic width Δ (or possibly a nonisotropic filter with widths Δ_i, $i=1,2,3$), obeys the dynamical equation (filtered Navier–Stokes equations),

$$\frac{\partial \tilde{u}_i}{\partial x_i}=0, \tag{1}$$

$$\frac{\partial \tilde{u}_i}{\partial t}+\tilde{u}_j\frac{\partial \tilde{u}_i}{\partial x_j}=-\frac{1}{\rho}\frac{\partial}{\partial x_j}\left(\frac{\tilde{p}}{\rho}\delta_{ij}+\tau_{ij}\right)+\nu\nabla^2\tilde{u}_i. \tag{2}$$

The anisotropic part of the SGS stress tensor is given by

$$\tau_{ij}\equiv\widetilde{u_iu_j}-\tilde{u}_i\tilde{u}_j-\tfrac{1}{3}\delta_{ij}(\widetilde{u_ku_k}-\tilde{u}_k\tilde{u}_k), \tag{3}$$

and the trace has been absorbed in the filtered pressure $\tilde{p}$. Also needed are the initial data $\tilde{u}_i(\mathbf{x},0)$ and boundary conditions on $\partial\Omega$. These are given by filtering the "real" initial and boundary conditions. For the discussion to follow, the field $\tilde{u}_i(\mathbf{x},t)$ is considered to be the "real" (not modeled) field, whose properties a velocity field computed through LES should strive to reproduce.

Now, let $u_i^*(\mathbf{x},t)$ be such a field resulting from a LES at a resolution similar to the filter-size considered before. It is divergence-free and is obtained by integration of the dynamical LES equation:

$$\frac{\partial u_i^*}{\partial t}+u_j^*\frac{\partial u_i^*}{\partial x_j}=-\frac{\partial}{\partial x_j}\left(\frac{p^*}{\rho}\delta_{ij}+\mathcal{T}_{ij}(\mathbf{u}^*)\right)+\nu\nabla^2u_i^*, \tag{4}$$

where $\mathcal{T}_{ij}(\mathbf{u}^*)$ is a model for the SGS stresses, expressed (closed) as a function of the resolved part of the velocity field. The functional dependence of $\mathcal{T}_{ij}$ on the field $\mathbf{u}^*$ is meant to be entirely general (i.e., it could, in principle, include dependence on the velocity at different points, any velocity gradients, the field at prior times, pressure gradients, etc., although subjected to general constraints such as Galilean invariance, causality, etc.). In this paper, we then consider the following question: What common statistical properties must τ_{ij}, the real SGS stresses, and $\mathcal{T}_{ij}(\mathbf{u}^*)$, the modeled ones, share in order to generate correct *statistical* features of the resolved velocity field.

Ideally, if the *entire* multiple point, multiple time, joint probability density of $\mathcal{T}_{ij}(\mathbf{u}^*)$ and $\mathbf{u}^*$ equals that of τ_{ij} and $\mathbf{u}$, then all statistical features of $\mathbf{u}^*$ should equal those of $\tilde{\mathbf{u}}$. However, accurate prediction of *all* statistics is probably too much to ask from a LES. A more useful set of questions is to find specific conditions that $\mathcal{T}_{ij}(\mathbf{u}^*)$ must obey in order to "cause" some low-order statistics of the LES velocity field to agree with the real statistics. Such questions are posed at several levels throughout the first part (Sec. II) of this paper: at the mean velocity level in Sec. II A, at the second-order level in Sec. II B, at the PDF level in Sec. II C and at the two-point statistics level in Sec. II D. In the second part of this paper (Sec. III), experimental data in grid turbulence is used for *statistical a priori* testing of several variants of the eddy viscosity model. In particular, a velocity-stress cross-correlation function relevant to the energy spectrum of the large-eddy field is measured and compared with predictions from the models. A summary, the final conclusions, and an outlook are presented in Sec. IV.

II. NECESSARY CONDITIONS FOR SGS STRESS STATISTICS

A. Mean flow

Here the following question is posed: What common statistical properties must the real SGS stresses τ_{ij} and the modeled ones $\mathcal{T}_{ij}(\mathbf{u}^*)$ share, in order to generate the correct ensemble average of the velocity field. To this end, it is instructive to perform an ensemble average of the filtered Navier–Stokes equations. This yields an equation for $\langle\tilde{u}_i\rangle$, the mean velocity field occurring in the real (filtered) flow,

$$\frac{\partial\langle\tilde{u}_i\rangle}{\partial t}+\langle\tilde{u}_j\rangle\frac{\partial\langle\tilde{u}_j\rangle}{\partial x_j}-\nu\nabla^2\langle\tilde{u}_i\rangle$$
$$=-\frac{\partial}{\partial x_j}\left(\frac{\langle\tilde{p}\rangle}{\rho}\delta_{ij}+(\langle\tilde{u}_i\tilde{u}_j\rangle-\langle\tilde{u}_i\rangle\langle\tilde{u}_j\rangle)+\langle\tau_{ij}\rangle\right). \quad (5)$$

The LES simulation, on the other hand, would yield a mean velocity field $\langle u_i^*\rangle$, which obeys the following version of the Reynolds equation [obtained from ensemble averaging Eq. (4)],

$$\frac{\partial\langle u_i^*\rangle}{\partial t}+\langle\tilde{u}_j^*\rangle\frac{\partial\langle u_j^*\rangle}{\partial x_j}-\nu\nabla^2\langle u_i^*\rangle$$
$$=-\frac{\partial}{\partial x_j}\left(\frac{\langle p^*\rangle}{\rho}\delta_{ij}+(\langle u_i^*u_j^*\rangle-\langle u_i^*\rangle\langle u_j^*\rangle)\right.$$
$$\left.+\langle\mathcal{T}_{ij}(\mathbf{u}^*)\rangle\right). \quad (6)$$

It can be noticed that the sum of the two stresses appearing on the RHS of these equations is nothing but the (filtered) Reynolds stress, i.e., the Germano identity[18] when the test "filter" is replaced by ensemble averaging. It is to be stressed that the model equation solved is *not* Eq. (6), but the original LES equation (4). Equation (6) is used here only to establish statistical properties of the solutions to Eq. (4). Inspection of Eqs. (5) and (6) immediately shows the following. For the modeled velocity and pressure field to exhibit the correct ensemble mean and the correct second-order moments, i.e., for the following equalities:

$$\langle u_i^*\rangle=\langle\tilde{u}_i\rangle,\quad \langle p^*\rangle=\langle\tilde{p}\rangle,$$
$$\langle u_i^*u_j^*\rangle=\langle\tilde{u}_i\tilde{u}_j\rangle,\quad \text{for all } \mathbf{x}\in\Omega, \quad (7)$$

to hold, the real and modeled mean stresses must be (up to an integration function) the same everywhere in Ω,

$$\langle\tau_{ij}\rangle=\langle\mathcal{T}_{ij}(\mathbf{u}^*)\rangle+C_{ij},\quad \mathbf{x}\in\Omega. \quad (8)$$

Here C_{ij} is an arbitrary divergence-free tensor (for instance, $\langle\tau_{ij}\rangle$ and $\langle\mathcal{T}_{ij}(\mathbf{u}^*)\rangle$ could differ by a constant value and still allow for the correct prediction of mean and second-order resolved moments). The condition of Eq. (8) is thus a necessary one for a LES simulation to yield *both* the correct mean and second-order moments (and mean pressure). However, it is not a sufficient condition. Even a model that yields the correct mean stress field could lead to an erroneous mean velocity field, if the "resolved" second-order moments are not correctly predicted.

Not much has been said so far about boundary conditions. Since what is being derived are necessary conditions, this is not too important. One can assume that the LES involved boundary conditions such that $\langle\mathbf{u}^*\rangle=\langle\tilde{\mathbf{u}}\rangle$ (or equality of gradients, etc.) is guaranteed on the boundary $\partial\Omega$. Since the focus is on necessary conditions, the issue about uniqueness of solutions to Eq. (6) does not play a role.

B. Second-order moments

A more useful result would have been to find, in the last section, that the equality of the real and modeled stresses is a *sufficient* condition for the equality of the mean velocity profiles. For this to be true, however, one must learn from a source different of Eqs. (5) and (6) that the second-order moments $\langle u_i^*u_j^*\rangle$ are the "correct" ones.

The second-order moments computed from the filtered velocity field obey

$$\frac{\partial}{\partial t}\langle\tilde{u}_i\tilde{u}_j\rangle+\langle\tilde{u}_k\rangle\frac{\partial}{\partial x_k}\langle\tilde{u}_i\tilde{u}_j\rangle-\nu\nabla^2\langle\tilde{u}_i\tilde{u}_j\rangle$$
$$=-\frac{\partial\Theta_{kij}}{\partial x_k}+Q_{ij}-\epsilon_{ij}-\Pi_{ij}. \quad (9)$$

Here

$$\Theta_{kij}=\rho^{-1}(\langle\tilde{p}\,\tilde{u}_i\rangle\delta_{jk}+\langle\tilde{p}\,\tilde{u}_j\rangle\delta_{ik})+(\langle\tilde{u}_k\tilde{u}_i\tilde{u}_j\rangle-\langle\tilde{u}_k\rangle\times\langle\tilde{u}_i\tilde{u}_j\rangle)+\langle\tilde{u}_i\tau_{jk}\rangle+\langle\tilde{u}_j\tau_{ik}\rangle, \quad (10)$$

causes transport of stress by correlations between resolved velocity fluctuations among themselves, with resolved pressure, as well as transport due to the unresolved motion

$$Q_{ij}=\frac{2}{\rho}\langle\tilde{p}\tilde{S}_{ij}\rangle\quad\left[\text{where } \tilde{S}_{ij}=\frac{1}{2}\left(\frac{\partial\tilde{u}_i}{\partial x_j}+\frac{\partial\tilde{u}_j}{\partial x_i}\right)\right], \quad (11)$$

is, as usual, a redistribution term due to resolved pressure–strain correlations;

$$\epsilon_{ij}=2\nu\left\langle\frac{\partial\tilde{u}_i}{\partial x_k}\frac{\partial\tilde{u}_j}{\partial x_k}\right\rangle \quad (12)$$

is the viscous dissipation tensor of the resolved field. Very importantly,

$$\Pi_{ij}=-(\langle\tilde{S}_{ik}\tau_{kj}\rangle+\langle\tilde{S}_{jk}\tau_{ki}\rangle) \quad (13)$$

is the loss term (whose trace represents the drain of resolved kinetic energy due to the SGS stress). An equation similar to Eq. (9) can be obtained for the modeled second-order moment $\langle u_i^*u_j^*\rangle$. Again, the question to be answered here is under what conditions can one expect the LES to yield the "correct" moments $\langle u_i^*u_j^*\rangle$. If such conditions could be found and be satisfied, then, according to the discussion in the last section, the equality of the mean stresses would be a sufficient condition to obtain the correct mean velocity field. Unfortunately, perusal of Eq. (9) (and its counterpart for the LES field) shows that one can only make a weaker statement, yielding an additional necessary condition on the stress statistics. One can now state this: In order for the LES to yield the following fields correctly: second- and third-order moments of resolved velocity, pressure velocity, pressure rate of strain correlation, *and* resolved dissipation tensor, one must ensure that the correlations between stresses and velocities, and between stresses and rate-of-strain tensor be the same in the "real" flow and in the LES one. Symbolically, to ensure that

$$\langle u_i^*\rangle=\langle\tilde{u}_i\rangle, \quad (14)$$
$$\langle u_i^*u_j^*\rangle=\langle\tilde{u}_i\tilde{u}_j\rangle;\quad \langle u_i^*u_j^*u_k^*\rangle=\langle\tilde{u}_i\tilde{u}_j\tilde{u}_k\rangle; \quad (15)$$

$$\langle p^* u_i^* \rangle = \langle \tilde{p}\, \tilde{u}_i \rangle; \quad \langle p^* S_{ij}^* \rangle = \langle \tilde{p} \tilde{S}_{ij} \rangle; \tag{16}$$

$$\left\langle \frac{\partial u_i^*}{\partial x_k} \frac{\partial u_j^*}{\partial x_k} \right\rangle = \left\langle \frac{\partial \tilde{u}_i}{\partial x_k} \frac{\partial \tilde{u}_j}{\partial x_k} \right\rangle, \tag{17}$$

the modeled stresses must exhibit the following correlations with the velocity field:

$$\langle S_{ik}^* \mathcal{T}_{kj}(\mathbf{u}^*) \rangle + \langle S_{jk}^* \mathcal{T}_{ki}(\mathbf{u}^*) \rangle - \frac{\partial}{\partial x_k} [\langle u_i^* \mathcal{T}_{jk}(\mathbf{u}^*) \rangle + \langle u_j^* \mathcal{T}_{ik}(\mathbf{u}^*) \rangle]$$
$$= \langle \tilde{S}_{ik} \tau_{kj} \rangle + \langle \tilde{S}_{jk} \tau_{ki} \rangle - \frac{\partial}{\partial x_k} (\langle \tilde{u}_i \tau_{jk} \rangle + \langle \tilde{u}_j \tau_{ik} \rangle). \tag{18}$$

Placing the additional requirement that a model should properly model SGS transport and SGS "dissipation" separately, we arrive at the conditions

$$\langle S_{ik}^* \mathcal{T}_{kj}(\mathbf{u}^*) \rangle + \langle S_{jk}^* \mathcal{T}_{ki}(\mathbf{u}^*) \rangle = \langle \tilde{S}_{ik} \tau_{kj} \rangle + \langle \tilde{S}_{jk} \tau_{ki} \rangle \tag{19}$$

and

$$\langle u_i^* \mathcal{T}_{jk}(\mathbf{u}^*) \rangle + \langle u_j^* \mathcal{T}_{ik}(\mathbf{u}^*) \rangle = \langle \tilde{u}_i \tau_{jk} \rangle + \langle \tilde{u}_j \tau_{ik} \rangle + C_{ij}, \tag{20}$$

where C_{ij} is again a divergence-free tensor (e.g., a constant). Specialization of these arguments to the fate of the kinetic energy ($i=j$) of the resolved motion in high Reynolds number, homogeneous and decaying turbulence, yields the condition that the correct rate of decay of energy can only be achieved if

$$\langle S_{mn}^* \mathcal{T}_{nm}(\mathbf{u}^*) \rangle = \langle \tilde{S}_{mn} \tau_{nm} \rangle, \tag{21}$$

i.e., if the model extracts energy at the correct rate. This is usually argued to be the main task of a subgrid model.

In summary, as one attempts to provide a sufficient condition for obtaining correct mean properties, new *necessary* conditions are generated that need to be obeyed by the stresses in order to obtain the correct first-, second-, and third-order statistics (and correlations with pressure) from the LES. Again, however, these alone are not sufficient to ensure correctness of second- and third-order moments.

C. PDF of resolved velocity

The preceding arguments can be carried to the more general level of the probability density function (PDF) of the resolved or modeled velocity field. One starts with the single-point PDF defined (see, e.g., Lundgren[19] and Pope[20]) as the ensemble average of the point probability, according to

$$f(\tilde{\mathbf{V}},\mathbf{x},t) \equiv \left\langle \prod_{i=1}^{3} \{\delta[\tilde{u}_i(\mathbf{x},t) - \tilde{V}_i]\} \right\rangle. \tag{22}$$

This is the joint PDF of the three velocity components, which may vary as a function of location and time. Starting from the filtered N–S equations and following Refs. 19 and 20, one can show that the evolution of $f(\tilde{\mathbf{V}},\mathbf{x},t)$ is given by the transport equation

$$\frac{\partial f}{\partial t} + \tilde{V}_j \frac{\partial f}{\partial x_j} = \frac{\partial}{\partial \tilde{V}_j} \left(f \left\langle \frac{1}{\rho} \frac{\partial \tilde{p}}{\partial x_j} + \frac{\partial \tau_{ij}}{\partial x_i} - \nu \nabla^2 \tilde{u}_j \middle| \tilde{\mathbf{u}} = \tilde{\mathbf{V}} \right\rangle \right). \tag{23}$$

The expression within brackets on the right represents the conditionally averaged force per unit mass acting on the filtered flow field at position $\mathbf{x}$. It consists of filtered pressure gradient, SGS, and viscous stresses, and it is conditioned upon the filtered velocity vector at the same point in question, at the same time. A similar expression is obtained for the PDF obtained through the LES, $f^*(\tilde{\mathbf{V}},\mathbf{x},t)$.

One can proceed further by expressing the pressure gradient as function of the velocity field in the entire domain Ω. Using the solution to the Poisson equation for filtered pressure and, for brevity's sake, assuming an unbounded domain, one obtains

$$\left\langle \frac{1}{\rho} \frac{\partial \tilde{p}}{\partial x_j} \middle| \tilde{\mathbf{u}} = \tilde{\mathbf{V}} \right\rangle = -\frac{1}{4\pi} \int_{\Omega} \frac{\partial^2}{\partial y_i \partial y_k} \langle \tilde{u}_i(\mathbf{y}) \tilde{u}_k(\mathbf{y}) + \tau_{ik}(\mathbf{y}) \,|\, \tilde{\mathbf{u}}(\mathbf{x}) = \tilde{\mathbf{V}} \rangle \frac{x_j - y_j}{|\mathbf{x}-\mathbf{y}|^3} d^3\mathbf{y}. \tag{24}$$

If the domain is bounded, surface integrals have to be included, but the nature of the discussion would be quite similar. Finally, expressing the conditional average of stress gradients as gradients of the two-point conditional average, we obtain

$$\frac{\partial f}{\partial t} + \tilde{V}_j \frac{\partial f}{\partial x_j} = \frac{\partial}{\partial \tilde{V}_j} \left[f \left(-\frac{1}{4\pi} \int_{\Omega} \frac{\partial^2}{\partial y_i \partial y_k} \times [\langle \tilde{u}_i(\mathbf{y}) \tilde{u}_k(\mathbf{y}) \,|\, \tilde{\mathbf{u}}(\mathbf{x}) = \tilde{\mathbf{V}} \rangle + \langle \tau_{ik}(\mathbf{y}) \,|\, \tilde{\mathbf{u}}(\mathbf{x}) = \tilde{\mathbf{V}} \rangle] \frac{x_j - y_j}{|\mathbf{x}-\mathbf{y}|^3} d^3\mathbf{y} + \lim_{\mathbf{y}\to\mathbf{x}} \frac{\partial}{\partial y_i} \langle \tau_{ij}(\mathbf{y}) \,|\, \tilde{\mathbf{u}}(\mathbf{x}) = \tilde{\mathbf{V}} \rangle - \nu \lim_{\mathbf{y}\to\mathbf{x}} \nabla_y^2 \langle \tilde{u}_j(\mathbf{y}) \,|\, \tilde{\mathbf{u}}(\mathbf{x}) = \tilde{\mathbf{V}} \rangle \right) \right]. \tag{25}$$

The PDF of the LES field obeys a similar equation, in which the stress is replaced by $\mathcal{T}_{ij}(\mathbf{u}^*)$. Examination of Eq. (25) now shows a necessary condition for achieving equality of the real and modeled PDF, as well as conditional two-point moments of resolved stresses and velocity. In other words, for the LES to generate

$$f^*(\tilde{\mathbf{V}},\mathbf{x},t) = f(\tilde{\mathbf{V}},\mathbf{x},t), \tag{26}$$

as well as

$$\langle u_i^*(\mathbf{y}) \,|\, \mathbf{u}^*(\mathbf{x}) = \tilde{\mathbf{V}} \rangle = \langle \tilde{u}_i(\mathbf{y}) \,|\, \tilde{\mathbf{u}}(\mathbf{x}) = \tilde{\mathbf{V}} \rangle, \tag{27}$$

and

$$\langle u_i^*(\mathbf{y}) u_k^*(\mathbf{y}) \,|\, \mathbf{u}^*(\mathbf{x}) = \tilde{\mathbf{V}} \rangle = \langle \tilde{u}_i(\mathbf{y}) \tilde{u}_k(\mathbf{y}) \,|\, \tilde{\mathbf{u}}(\mathbf{x}) = \tilde{\mathbf{V}} \rangle, \tag{28}$$

at least the following condition must be met:

$$-\frac{1}{4\pi}\int_\Omega \frac{\partial^2}{\partial y_i \partial y_k}\langle \mathscr{T}_{ik}(\mathbf{y})\,|\,\mathbf{u}^*(\mathbf{x})=\tilde{\mathbf{V}}\rangle \frac{x_j-y_j}{|\mathbf{x}-\mathbf{y}|^3}\,d^3\mathbf{y}$$
$$+\lim_{\mathbf{y}\to\mathbf{x}}\frac{\partial}{\partial y_i}\langle \mathscr{T}_{ij}(\mathbf{y})\,|\,\mathbf{u}^*(\mathbf{x})=\tilde{\mathbf{V}}\rangle$$
$$=-\frac{1}{4\pi}\int_\Omega \frac{\partial^2}{\partial y_i \partial y_k}\langle \tau_{ik}(\mathbf{y})\,|\,\tilde{\mathbf{u}}(\mathbf{x})=\tilde{\mathbf{V}}\rangle$$
$$\times\frac{x_j-y_j}{|\mathbf{x}-\mathbf{y}|^3}\,d^3\mathbf{y}+\lim_{\mathbf{y}\to\mathbf{x}}\frac{\partial}{\partial y_i}\langle \tau_{ij}(\mathbf{y})\,|\,\tilde{\mathbf{u}}(\mathbf{x})=\tilde{\mathbf{V}}\rangle+C_j. \tag{29}$$

Here C_j is an integration constant, divergence-free with respect to $\tilde{\mathbf{V}}$. As can be seen, analysis of conditions for the single-point PDF have yielded conditions involving two-point conditional statistics of the SGS stress. In particular, the above condition would be satisfied if one can show that

$$\langle \tau_{ik}(\mathbf{y})\,|\,\tilde{\mathbf{u}}(\mathbf{x})=\tilde{\mathbf{V}}\rangle = \langle \mathscr{T}_{ik}[\mathbf{u}^*(\mathbf{y})]\,|\,\mathbf{u}^*(\mathbf{x})=\tilde{\mathbf{V}}\rangle, \quad \forall \mathbf{y},\mathbf{x}\in\Omega. \tag{30}$$

Berkooz[21] examines similar questions based on the PDF equation of dynamical systems. He proposes a method for constructing new models based on appropriate moments of full simulations, and has applied the procedure to the Lorentz equations.

1. Velocity PDFs in isotropic turbulence

For the special case of isotropic turbulence, the condition in Eq. (30) can be cast in terms of a few scalar functions. The conditional average is a trace-free symmetric tensor depending on two vectors, $\mathbf{r}=\mathbf{y}-\mathbf{x}$ and $\tilde{\mathbf{V}}$. It must then take the form

$$\langle \tau_{ik}(\mathbf{y})\,|\,\tilde{\mathbf{u}}(\mathbf{x})=\tilde{\mathbf{V}}\rangle = Ar_ir_j+B\tilde{V}_i\tilde{V}_j+C(r_i\tilde{V}_j+r_j\tilde{V}_i) -\tfrac{1}{3}(Ar^2+B\tilde{V}^2+2C\mathbf{r}\cdot\tilde{\mathbf{V}})\delta_{ij}. \tag{31}$$

Here A, B, and C are scalar functions of r, $\tilde{V}$, and $\mathbf{r}\cdot\tilde{\mathbf{V}}$. They can be expressed in terms of three conditional averages involving longitudinal (L) and normal (N) directions. A possible choice appears below,

$$A=\frac{2\langle \tau_{LL}(r_L)\,|\,\tilde{V}_N\rangle+\langle \tau_{NN}(r_L)\,|\,\tilde{V}_N\rangle}{r_L^2}, \tag{32}$$

$$B=\frac{2\langle \tau_{NN}(r_L)\,|\,\tilde{V}_N\rangle+\langle \tau_{LL}(r_L)\,|\,\tilde{V}_N\rangle}{\tilde{V}_L^2}, \tag{33}$$

and

$$C=\frac{\frac{3}{4}\langle \tau_{LL}(r_L)\,|\,\tilde{V}_L\rangle-3\langle \tau_{LL}(r_L)\,|\,\tilde{V}_N\rangle-3\langle \tau_{NN}(r_L)\,|\,\tilde{V}_N\rangle}{r_L\tilde{V}_L}. \tag{34}$$

Here, expressions of the type $\langle \tau_{mn}(r_j)\,|\,\tilde{V}_k\rangle$ stand for the conditional average of the mn stress-stensor element at a distance r in the j direction from a point where the resolved velocity has magnitude $\tilde{V}$ in the k direction. These three functions (of two independent variables each) needed to completely specify the two-point conditional stress average in isotropic turbulence are illustrated in Fig. 1.

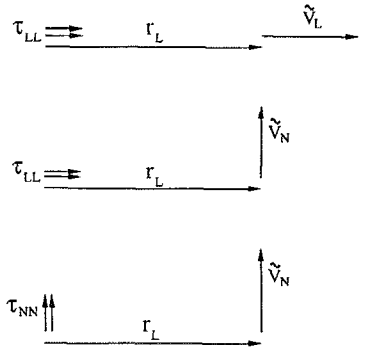

FIG. 1. Sketch of relevant directions of conditionally averaged SGS stress tensor in isotropic turbulence. Three scalar functions, each depending on two arguments (distance and velocity magnitude) are needed to completely describe the conditional mean SGS stress.

D. Two-point statistics

Here we shall focus on two-point second-order moments of the resolved fields in homogeneous turbulence.

1. Correlation functions

We define the resolved (real and modeled) two-point velocity correlation tensor as

$$B_{ij}(\mathbf{r},t)\equiv\langle \tilde{u}_i\tilde{u}'_j\rangle; \quad B^*_{ij}(\mathbf{r},t)\equiv\langle u^*_i u'^*_j\rangle. \tag{35}$$

The prime indicates that the velocity is evaluated at point $\mathbf{x}+\mathbf{r}$ instead of $\mathbf{x}$. As usual, the filtered Navier–Stokes equations are now multiplied by the filtered velocity at the second point, leading to

$$\left(\frac{\partial}{\partial t}-2\nu\nabla_r^2\right)B_{ij}(\mathbf{r})=\frac{1}{\rho}\frac{\partial}{\partial r_i}\langle p\tilde{u}'_j\rangle-\frac{1}{\rho}\frac{\partial}{\partial r_j}\langle p'\tilde{u}_i\rangle +\frac{\partial}{\partial r_k}(B_{ik,j}+B_{jk,i}) +\frac{\partial}{\partial r_k}(G_{ik,j}+G_{jk,i}). \tag{36}$$

Here

$$B_{ik,j}(\mathbf{r},t)=\langle \tilde{u}_i\tilde{u}_k\tilde{u}'_j\rangle; \quad G_{ik,j}(\mathbf{r},t)=\langle \tilde{u}'_j\tau_{ik}\rangle. \tag{37}$$

To simplify the exposition, we now consider isotropic turbulence. The correlations with pressure vanish (see, e.g., Monin and Yaglom, 1975[22]) and the remaining tensors can be expressed in terms of a few scalar functions. We consider longitudinal correlation functions, i.e.,

$$B_{LL}(r,t)\equiv\langle \tilde{u}_L(\mathbf{x},t)\tilde{u}_L(\mathbf{x}+\mathbf{r}_L,t)\rangle, \tag{38}$$

where $\mathbf{r}_L$ is the separation vector in the L direction, and whose magnitude is r. Also,

$$B_{LLL}(r,t)\equiv\langle \tilde{u}_L(\mathbf{x},t)^2\tilde{u}_L(\mathbf{x}+\mathbf{r}_L,t)\rangle; \quad G_{LLL}(r,t)\equiv\langle \tau_{LL}(\mathbf{x},t)\tilde{u}_L(\mathbf{x}+\mathbf{r}_L,t)\rangle \tag{39}$$

are the longitudinal third-order correlation functions. The evolution of the longitudinal correlation function $B_{LL}(r,t)$ is given by

$$\left[\frac{\partial}{\partial t}-2\nu\left(\frac{\partial^2}{\partial r^2}+\frac{4}{r}\frac{\partial}{\partial r}\right)\right]B_{LL}(r,t)-\left(\frac{\partial}{\partial r}+\frac{4}{r}\right)B_{LLL}(r,t)$$

$$=\left(\frac{\partial}{\partial r}+\frac{4}{r}\right)G_{LLL}(r,t). \tag{40}$$

This is the von Kármán–Howarth equation for the resolved portion of the velocity field, in which the third-order correlations are decomposed into those arising from the resolved field, B_{LLL}, and those coming from the interactions with the subgrid scales, G_{LLL} (also see the discussion by Leonard, 1974[23]). A similar equation governs the evolution of the LES correlations, involving $B^*_{LL}(r,t)$, $B^*_{LLL}(r,t)$, and $G^*_{LLL}(r,t)$.

As in the previous sections, we can make the following type of statement: In order for the SGS model to generate *both* the correct correlation functions $B_{LL}(r,t)$ and the correct resolved third-order correlations B_{LLL}, one must ensure that the scalar function G_{LLL} is predicted correctly. In other words, to allow for the following equalities:

$$B_{LL}(r,t)=B^*_{LL}(r,t);\quad B_{LLL}(r,t)=B^*_{LLL}(r,t), \tag{41}$$

a necessary condition is that

$$G_{LLL}(r,t)=G^*_{LLL}(r,t). \tag{42}$$

Notice that an arbitrary integration function [obeying $(\partial/\partial r+4/r)C(r)=0$] does not enter here, because it would diverge at $r=0$. Again, however, Eq. (42) by itself is not a sufficient condition to ensure the correct correlation functions B_{LL} and B_{LLL}.

2. A sufficient condition for structure functions in locally isotropic turbulence

We now define the longitudinal structure functions,

$$\tilde{D}_{LL}\equiv\langle[\tilde{u}_L(\mathbf{x}+\mathbf{r}_L)-\tilde{u}_L(\mathbf{x})]^2\rangle$$

$$=2[B_{LL}(0,t)-B_{LL}(r,t)] \tag{43}$$

and

$$\tilde{D}_{LLL}\equiv\langle[\tilde{u}_L(\mathbf{x}+\mathbf{r}_L)-\tilde{u}_L(\mathbf{x})]^3\rangle=6B_{LLL}(r,t). \tag{44}$$

Evaluating Eq. (40) at $r=0$ and using $\partial G_{LLL}/\partial r=\langle\tilde{S}_{LL}(\mathbf{x}+\mathbf{r}_L)\tau_{LL}(\mathbf{x})\rangle$ (where $\tilde{S}_{LL}$ is the longitudinal component of the filtered velocity rate-of-strain tensor) yields

$$\frac{\partial}{\partial t}B_{LL}(0,t)=5(2\nu B''_{LL}(0,t)+\langle\tilde{S}_{LL}\tau_{LL}\rangle). \tag{45}$$

This result is replaced in Eq. (40), written in terms of structure functions. As usual, one argues that for r much smaller than the flow-integral scale, the rate of change of $\tilde{D}_{LL}(r,t)$ in time is negligible compared to the other terms. After integration, one obtains

$$\tfrac{1}{6}\tilde{D}_{LLL}+\langle u_L(\mathbf{x}+\mathbf{r}_L)\tau_{LL}(\mathbf{x})\rangle-\nu\tilde{D}'_{LL}$$

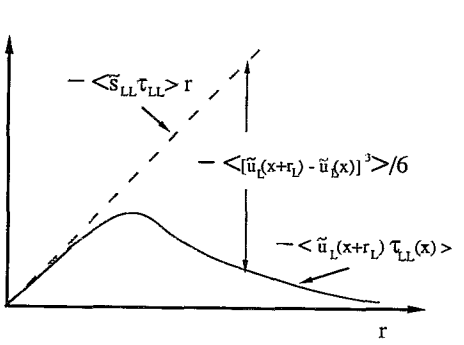

FIG. 2. Sketch of various terms appearing in the equation for the resolved longitudinal structure function in locally isotropic turbulence, as a function of displacement.

$$=(2\nu B''_{LL}(0)+\langle\tilde{S}_{LL}\tau_{LL}\rangle)r. \tag{46}$$

For high Reynolds numbers (and $\Delta\gg\eta$), this becomes

$$\langle[\tilde{u}_L(\mathbf{x}+\mathbf{r}_L)-\tilde{u}_L(\mathbf{x})]^3\rangle+6\langle\tilde{u}_L(\mathbf{x}+\mathbf{r}_L)\tau_{LL}(\mathbf{x})\rangle$$

$$=6\langle\tilde{S}_{LL}\tau_{LL}\rangle r. \tag{47}$$

This relation is quite interesting and falls somewhat outside the hierarchy previously encountered: If the two-point correlation function $G_{LLL}=\langle u_L(\mathbf{x}+\mathbf{r}_L)\tau_{LL}(\mathbf{x})\rangle$ is correctly modeled, then it must lead to the correct third-order structure function (recalling that $\langle\tilde{S}_{LL}\tau_{LL}\rangle$ is just G'_{LLL} at $r=0$). In other words, this now provides a *sufficient* condition under the assumptions made during the derivation.

At very small r, $\tilde{D}_{LLL}\sim r^3$. Therefore the correlation $\langle\tilde{u}_L(\mathbf{x}+\mathbf{r}_L)\tau_{LL}(\mathbf{x})\rangle$ must be linear in r, with slope $\langle\tilde{S}_{LL}\tau_{LL}\rangle$. At large $r\gg\Delta$, but still within the inertial range, one expects the structure function to be linear in r and the velocity-stress cross correlation to become small. The expected trends of these terms is illustrated in Fig. 2.

Expanding Eq. (47) in powers of r for small r, yields the balance of energy dissipation at the order r^1. The next term is of order r^3 and relates the third-order moment of filtered velocity derivatives to the SGS stresses, according to

$$\left\langle\left(\frac{\partial\tilde{u}_L}{\partial x_L}\right)^3\right\rangle=-\left\langle\frac{\partial^3\tilde{u}_L}{\partial x_L^3}\tau_{LL}\right\rangle. \tag{48}$$

This equality describes the equilibrium between production of enstrophy of the resolved field and dissipation of resolved-scale enstrophy by the SGS stresses. As always, a similar expression can be written down for the field resulting from the LES:

$$\left\langle\left(\frac{\partial u^*_L}{\partial x_L}\right)^3\right\rangle=-\left\langle\frac{\partial^3 u^*_L}{\partial x_L^3}\mathscr{T}_{LL}(\mathbf{u}^*)\right\rangle. \tag{49}$$

This shows that a sufficient condition for obtaining the correct third-order moment of velocity gradients from the LES is to properly model the correlation

$$\left\langle\frac{\partial^3\tilde{u}_L}{\partial x_L^3}\tau_{LL}\right\rangle=\left\langle\frac{\partial^3 u^*_L}{\partial x_L^3}\mathscr{T}_{LL}[\mathbf{u}^*]\right\rangle. \tag{50}$$

In order to generalize this condition to nonisotropic turbulence, it is straightforward to consider the resolved vorticity equation containing the SGS stress tensor. After contracting with $\tilde{\omega}_i$ (the resolved vorticity), one obtains an equation for the resolved enstrophy:

$$\frac{\partial(\tilde{\omega}_i^2/2)}{\partial t}+\tilde{u}_j\frac{\partial(\tilde{\omega}_i^2/2)}{\partial x_j}=\tilde{\omega}_i\tilde{\omega}_j\tilde{S}_{ij}+\nu\tilde{\omega}_i\nabla^2\tilde{\omega}_i-2\tilde{R}_{jk}\frac{\partial^2\tau_{lj}}{\partial x_k\partial x_l}, \tag{51}$$

where $\tilde{R}_{ij}=-\epsilon_{ijk}\tilde{\omega}_k/2$ is the rotation tensor. Taking the ensemble average, assuming statistical stationarity and a high-Reynolds number, Eq. (48) is generalized to

$$\langle\tilde{\omega}_i\tilde{\omega}_j\tilde{S}_{ij}\rangle=\left\langle 2\tilde{R}_{jk}\frac{\partial^2\tau_{lj}}{\partial x_k\partial x_l}\right\rangle=2\left\langle\tau_{lj}\frac{\partial^2\tilde{R}_{jk}}{\partial x_k\partial x_l}\right\rangle, \tag{52}$$

where the last equality holds for homogeneous flows. Some comments on possible applications of this relation to formulate an "enstrophy SGS model" are given in Sec. III when analyzing experimental results.

Returning to isotropic turbulence, the next term in the expansion of Eq. (47) (describing equilibrium between production and "dissipation" of palenstrophy) arises at order r^5 and reads as

$$\left\langle\left(\frac{\partial^2\tilde{u}_L}{\partial x_L^2}\right)^2\left(\frac{\partial\tilde{u}_L}{\partial x_L}\right)\right\rangle=-\frac{1}{30}\left\langle\frac{\partial^5\tilde{u}_L}{\partial x_L^5}\tau_{LL}\right\rangle. \tag{53}$$

This can be continued to higher-order coefficients in the expansion, every time obtaining a more stringent statistical condition that the modeled SGS tensor needs to obey, as a sufficient condition for obtaining the correct higher-order-derivative moment of the LES velocity field.

E. Statistical *a priori* testing

The statements made in Secs. II A–II D can be understood as the identification of measureable quantities of interest in the study and testing of SGS models. For *statistical a priori* testing of models, moments (and joint statistics with the resolved velocity) of the SGS stresses computed from a fully resolved field $\mathbf{u}$ (DNS or experimental) are compared to the predictions of a particular model. The goal is to test whether a given model can match the necessary conditions introduced in Secs. II A–II D.

The discussion of the previous sections refers to comparison between statistical measures of τ_{ij} and $\mathcal{T}_{ij}(\mathbf{u}^*)$. To evaluate the latter, however, it was understood that the LES field $\mathbf{u}^*$ was known. On the other hand, in order for the *a priori* test to be practical, it should be based on the measured field $\mathbf{u}$ only and not require an additional LES computation. Otherwise, one may as well perform *a posteriori* testing and directly compare statistics of $\tilde{\mathbf{u}}$ to those of $\mathbf{u}^*$. So, what one really wishes to compare is τ_{ij} and $\mathcal{T}_{ij}(\tilde{\mathbf{u}})$. For instance, in order to find necessary conditions to correctly predict the mean velocity, pressure, and second moments in a LES, one would measure $\langle\tau_{ij}\rangle$ and $\langle\mathcal{T}_{ij}(\tilde{\mathbf{u}})\rangle$ instead of $\langle\mathcal{T}_{ij}(\mathbf{u}^*)\rangle$. This means that besides the conditions spelled out in Sec. II A, an additional assumption must now be made, namely, that

$$\langle\mathcal{T}_{ij}(\tilde{\mathbf{u}})\rangle=\langle\mathcal{T}_{ij}(\mathbf{u}^*)\rangle. \tag{54}$$

Alternatively, the necessary condition derived in terms of the equality of real and modeled SGS stress is a necessary one for equality of mean, second-order velocity moments (as before), *and* the equality of the statistical expression resulting from the model. This statement is easier to understand through an illustrative example: Assume that the Smagorinsky model is being studied by *a priori* testing using DNS of some particular nonhomogeneous flow field, say, a channel flow [see, e.g., Ref. 11, Fig. 2]. Now, the stresses τ_{ij} are computed by filtering the DNS field $\mathbf{u}$ at some length scale Δ (larger than the original grid). Also, the "modeled" stresses are calculated according to $-2C_s^2\Delta^2(2\tilde{S}_{mn}\tilde{S}_{mn})^{1/2}\tilde{S}_{ij}$. Ensemble average values of both stress tensors are calculated as time averages or over homogeneous spatial directions. This can lead to two different results (a) The average real and modeled SGS stresses are equal to each other at every point in the flow or (b) they differ. In case (b), one can conclude that it is not possible for a LES to reproduce simultaneously the mean flow, mean pressure, the second-order moments *and* the "Smagorinsky moment" $\langle(\tilde{S}_{mn}\tilde{S}_{mn})^{1/2}\tilde{S}_{ij}\rangle$. In the case (a) that the mean stresses agree everywhere, one can conclude that it is *possible* for the mean velocity, mean pressure, second-order, and Smagorinsky moments to be correctly generated by a LES. However, (a) does not *imply* that these moments will be correct because, as remarked before, errors in the mean flow could instead be generated by erroneous second-order moments, or now, by different values of the "Smagorinsky moment," i.e. $\langle(\tilde{S}_{mn}\tilde{S}_{mn})^{1/2}\tilde{S}_{ij}\rangle\neq\langle(S^*_{mn}S^*_{mn})^{1/2}S^*_{ij}\rangle$.

If one is not satisfied at this particular level, one can proceed to second-order moments and compare the rate-of-strain stress correlation at every point. If they agree, then it is possible that the second-order moments would be correctly predicted (although, again, this is not guaranteed), increasing the likelihood that the correct mean flow would be obtained from the LES.

Such a statistical study of several eddy-viscosity models is performed in the next section.

III. EXPERIMENTAL TESTS IN GRID TURBULENCE

In previous sections the importance of several statistical properties of the SGS stress tensor have been pointed out. In this section we analyze experimental data obtained in (nearly) isotropic flow (grid turbulence) from a single hot wire. This simple flow is chosen here as a starting point. Applications to nonisotropic shear flows, more specialized tests, and more complete experimental data will be reported elsewhere.[17,24] In isotropic turbulence the mean stresses are zero, so nothing interesing occurs at the level of mean quantities. Thus, we proceed to the level of energy dynamics and two-point statistics. The necessity of correctly predicting the stress-velocity cross-correlation,

$$\langle\tilde{u}_L(\mathbf{x}+\mathbf{r}_L)\tau_{LL}(\mathbf{x})\rangle=\langle\tilde{u}_L(\mathbf{x}+\mathbf{r}_L)\mathcal{T}_{LL}[\mathbf{u}(\tilde{\mathbf{x}})]\rangle, \tag{55}$$

has been highlighted (Sec. II D). This condition is necessary to obtain the correct resolved energy spectrum from a

LES of isotropic turbulent flow, and is sufficient for the prediction of third-order structure functions.

Three variants of the eddy-viscosity SGS closure are studied. They are tested by evaluating SGS energy and enstrophy fluxes, as well as by measuring both sides of expression (55). Measurements from a single hot-wire probe, along with Taylor's hypothesis, are employed. Thus, only $u_1(x_1)$ is available for the analysis. As will be described in more detail when appropriate, this forces us to proceed by (a) filtering in only a single direction x_1, instead of all three; (b) evaluating local eddy viscosities based on single components; and (c) not subtracting the trace of the SGS stress tensor. The impact of step (a) will be quantified in the Appendix and step (c) will be shown to be of no relevance for isotropic turbulence. Step (b), although more difficult to justify, will *a posteriori* be argued to have little impact on the results. Therefore, although these procedures are expected to alter some quantitative results, the working hypothesis is that the observed *trends* obtained through such an analysis are representative of the real trends.

The details on the experimental setup and data processing are given in Secs. III A and III B. Some general results are presented in Sec. III C and model constants are studied in Secs. III D 1, III D 2, and III D 3. The results on the velocity-stress cross-correlation function are presented in Sec. III E.

A. Experimental conditions and flow characterization

Measurements were performed in a closed loop, low-speed, wind tunnel with a $0.91\times1.22\times10$ m test section. The location of the probe was at $x/M=68.7$ downstream of a grid (square bars, 1.9 cm thick), with mesh size $M=10.2$ cm. Also, a secondary 1:1.27 contraction[25] was used to promote component isotropy. The mean velocity was $U=25.2$ m/s, the longitudinal integral scale was $L_1=8.3$ cm, the root-mean-square streamwise velocity was $u_1'=0.42$ m/s, and the Taylor-scale Reynolds number was $R_\lambda\sim170$. A 0.45 mm long Dantec-A53 subminiature probe and a Dantec-56C17 anemometer were operated at an overheat ratio of 1.8. After low-pass filtering at $f_c=30$ kHz, the signal was digitized on a 12 bit A/D board at a sampling frequency of $f_s=60$ kHz. Some additional digital filtering is employed to eliminate high-frequency noise peaks. More details on the experimental setup and signal conditioning are given in Ref. 26.

A total of 3×10^6 samples are analyzed, and all quantities computed are statistically fully converged. The dissipation rate, estimated from the isotropy relation,

$$\langle\epsilon\rangle=15\nu\left\langle\left(\frac{\partial u_1}{\partial x_1}\right)^2\right\rangle, \tag{56}$$

is $\langle\epsilon\rangle=1.15$ m^2/s^3. Taylor's hypothesis is used,

$$\frac{\partial}{\partial x_1}=-\frac{1}{U}\frac{\partial}{\partial t}, \tag{57}$$

and time derivatives are computed with a simple finite difference of the consecutive samples. The Kolmogorov scale is $\eta=0.23$ mm, smaller than the probe length by a factor of about $l/\eta=2$. The skewness of the velocity derivative is -0.38. The energy spectrum normalized in Kolmogorov units is shown in Fig. 3, alongside other experimental data. Although the inertial range is very small, the collapse on the universal curve is good. The normalized third-order velocity structure function $\langle[u_1(x+r)-u_1(x)]^3\rangle/(\langle\epsilon\rangle r)$ is shown in Fig. 4. While no extended inertial range exists at this moderate Reynolds number, the peak is not too far from the asymptotic $-\frac{4}{5}$ value for isotropic turbulence. The skewness of the velocity itself is $\langle u_1^3\rangle/\langle u_1^2\rangle^{3/2}=0.033$, which is small (although for perfectly isotropic turbulence one would expect this value to be zero).

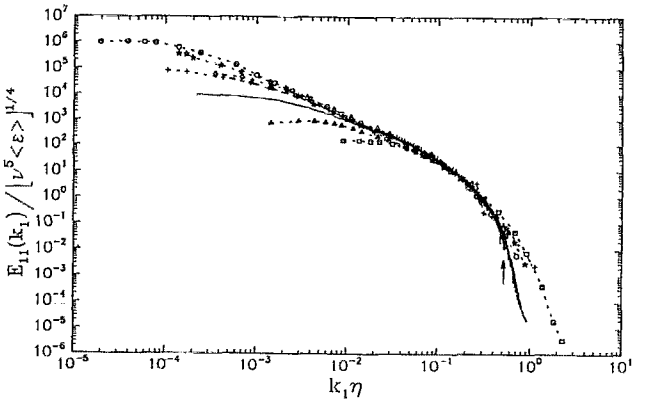

FIG. 3. Solid line: Measured longitudinal energy spectrum of the grid turbulence data ($R_\lambda\sim170$) used for the present analysis, in Kolmogorov units. The rapid rolloff seen at $k_1\eta>0.5$ is due to the filtering employed to eliminate noise as well as to probe resolution. Symbols are a representative compilation from other experimental data: Squares: grid turbulence $R_\lambda=37$ (Comte-Bellot and Corrsin, 1971); triangles: grid turbulence $R_\lambda=72$ (Comte-Bellot and Corrsin, 1971); plus: cylinder wake $R_\lambda=308$ (Uberoi and Freymuth, 1969); rhombs: grid turbulence $R_\lambda=540$ (Kistler and Vrebalovich, 1966); stars: round jet $R_\lambda=780$ (Gibson, 1963); circles: boundary layer $R_\lambda=1{,}450$ (recent data of Veeravalli and Saddoughi, Ref. 27, 1991).

B. Data processing and models

1. Filters

Several filters are employed to compute the "resolved" velocity $\tilde{u}_1(x)$ at scale Δ,

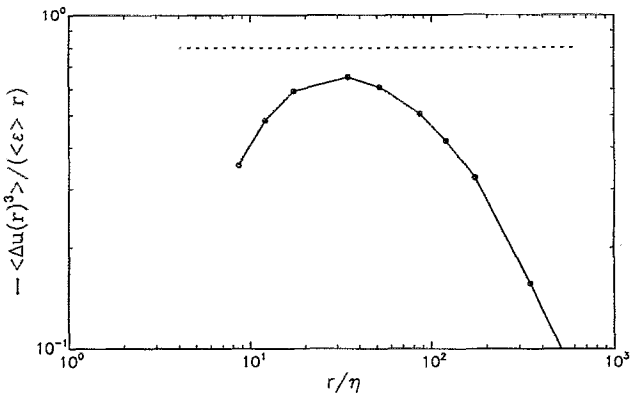

FIG. 4. Dimensionless third-order structure function.

$$\tilde{u}_1(x)=\int_{-\infty}^{\infty} u_1(x_1')F_\Delta(x_1-x_1')dx_1'. \tag{58}$$

This is done using FFT, using zero padding (statistics were later evaluated only over points unaffected by end effects). Similar expressions are used to compute the stress element τ_{11}.

Cutoff, Gaussian, and top-hat filters are considered. The cutoff filter is used to generate resolved fields that mimic those available during a LES using a spectral method, while a top-hat filter may be more in line with a finite-difference scheme (although this correspondence is not at all exact[27]). The Gaussian filter, being of intermediate resolution in physical and wave number space, may produce resolved fields containing information similar to that of a LES using a (hypothetical) wavelet method. Since the compatibility between a numerical method and corresponding filter type is presently not well understood, the above-mentioned relations have to be regarded with caution.

The filters employed are one dimensional: no filtering is performed in the x_2 and x_3 directions. The reason for this approach is simply lack of experimental data, except along a line in the x_1 direction (using Taylor's hypothesis). For now, the working hypothesis is that the one-dimensional (1-D) filtered quantities do not appreciably differ from their (3-D) counterparts, as far as the observed trends in the measured statistics is concerned. In the Appendix it is shown, based on an inertial range evaluation of the Smagorinsky constant, that this assumption cannot hold exactly, especially as far as the correlation $\langle \tilde{S}_{pq}\tilde{S}_{pq}\rangle$ is concerned. Moreover, nonisotropic filtering of an isotropic field $\mathbf{u}$ produces anisotropy in $\tilde{\mathbf{u}}$, especially for two-point correlations at small separations $r<\Delta$. However, we continue to employ the working hypothesis to argue that observed *trends* should be realistic. Alternatively, the Appendix introduces a more precise interpretation of the present analysis in terms of anisotropic filtering relevant to LES on highly anisotropic meshes.

The filters employed are

$$\text{Cutoff:}\quad F_\Delta(x_1)=\frac{\sin(\pi x_1/\Delta)}{\pi x_1/\Delta}; \tag{59}$$

$$\text{Gaussian:}\quad F_\Delta(x_1)=\sqrt{\frac{6}{\Pi}}\frac{1}{\Delta}\exp\left(-\frac{6x_1^2}{\Delta^2}\right), \tag{60}$$

$$\text{Top hat:}\quad F_\Delta(x_1)=\frac{1}{\Delta},\quad \text{if } |x_1|<\frac{\Delta}{2},$$

$$F_\Delta(x_1)=0 \text{ otherwise.} \tag{61}$$

These filters and their transfer function in Fourier space are shown in Fig. 5.

The τ_{11} element of the total SGS stress tensor is computed according to

$$\tau_{11}(x_1)=\widetilde{u_1u_1}-\tilde{u}_1\tilde{u}_1, \tag{62}$$

where again the overtilde denotes filtering with F_Δ. Notice that the trace has not been subtracted, since we are not performing simultaneous measurements of u_2 and u_3. For

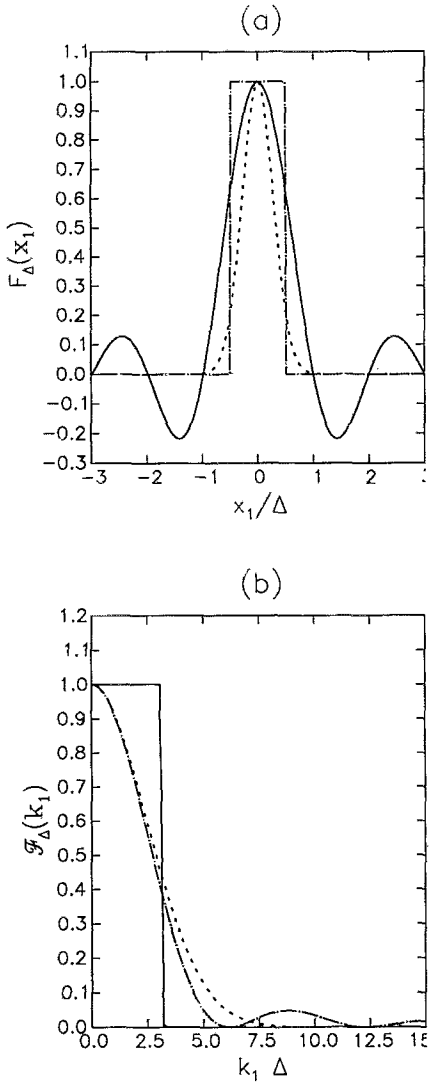

FIG. 5. Shape of filters used in the analysis of data. (a) $F_\Delta(x_1)$ in physical space (prior to normalization to unit area), ——: cutoff; ···: Gaussian; - · -: top hat. (b) Transfer function in Fourier space $\hat{F}_\Delta^2(k)$, ——: cutoff; ···: Gaussian; - · -: top hat.

evaluating the stress-velocity correlation in isotropic turbulence, this is of no concern, as seen below. The correlation involving the trace of the stress is a vector that only depends on $\mathbf{r}$:

$$\langle \tau_{pp}(\mathbf{x})\tilde{u}_i(\mathbf{x}+\mathbf{r})\rangle=C(|r|)r_i=0. \tag{63}$$

The last equality follows from taking the divergence with $\mathbf{r}$ and using incompressibility. Therefore

$$\langle(\tau_{11}(\mathbf{x})-\tfrac{1}{3}\tau_{pp}(\mathbf{x}))\tilde{u}_1(\mathbf{x}+\mathbf{r})\rangle=\langle\tau_{11}(\mathbf{x})\tilde{u}_1(\mathbf{x}+\mathbf{r})\rangle. \tag{64}$$

Similar arguments hold for the correlation $\langle\tilde{S}_{ij}\tau_{pp}\rangle$, which must vanish because it is a traceless isotropic tensor. Therefore

$$\langle\tilde{S}_{11}(\tau_{11}-\tfrac{1}{3}\tau_{pp})\rangle=\langle\tilde{S}_{11}\tau_{11}\rangle. \tag{65}$$

2. Eddy viscosity models

Several eddy viscosity models of the form,

$$\mathcal{T}_{ij}[\tilde{\mathbf{u}}] = -2\nu_T \tilde{S}_{ij}, \tag{66}$$

are considered. The first is the usual Smagorinsky eddy viscosity. Instead of using the complete second invariant of the rate-of-strain tensor (because of present limitations in measurements), a one-dimensional surrogate is employed, assuming instantaneous isotropy:

$$\mathcal{T}_{11}^{(1)}[\tilde{u}_1] = -2(C_1\Delta)^2 \sqrt{15(\tilde{S}_{11})^2}\tilde{S}_{11}. \tag{67}$$

The second model is a constant eddy viscosity assumption, using the global average instead of the local value of the rate of strain:

$$\mathcal{T}_{11}^{(2)}[\tilde{u}_1] = -2(C_2\Delta)^2 \sqrt{15\langle(\tilde{S}_{11})^2\rangle}\tilde{S}_{11}. \tag{68}$$

This model is considered for the purpose of exploring the influence of eddy-viscosity fluctuations on the resulting statistics. It is understood that in a simulation the numerical value of the eddy viscosity would be obtained from the resolved field by averaging over homogeneous directions, time, etc. This model actually resembles the (wave number-independent) spectral eddy-viscosity closures, where the eddy viscosity is evaluated, based on the computed energy spectrum at the cutoff. Thus, it differs from a "constant eddy-viscosity" model in which a particular numerical value is assumed *a priori* for the eddy viscosity.

As a third model we obtain the velocity scale based on the SGS kinetic energy:

$$q^2 = 3(u_1 - \tilde{u}_1)^2, \tag{69}$$

$$\mathcal{T}_{11}^{(3)}[\tilde{u}_1] = -2C_3^2\Delta \sqrt{|\tilde{q}^2|}\tilde{S}_{11}, \tag{70}$$

again based on the u_1 values only. For this model, an additional transport equation for $\tilde{q}^2$ is envisioned, as in Refs. 29 and 30. For now, we assume $\tilde{q}^2$ to be known and concentrate on expression (70).

The modeled stress elements are computed over the entire data set. A representative segment of the real stress τ_{11} and the modeled ones (without multiplying them by the model constants) are shown in Figs. 6–8, for the Gaussian filter with $\Delta = 32\eta$. Note that no direct comparison between the two signals is possible, because the trace has not been subtracted from $\tau_{11}(x_1)$. This causes that signal to be strictly positive, whereas the model expression displays both signs. [Note that for the cutoff filter one occasionally encounters $\tau_{11}(x_1) < 0$; this is also the reason that the absolute value is taken inside the square root in Eq. (70).] As has been argued before, not subtracting the trace should not influence the statistics of interest, in grid turbulence. However, it could influence the observations that follow. We notice a fairly good correspondence between peaks in $\tau_{11}(x_1)$ and $\mathcal{T}_{11}(x_1)$: However, since the sign of the excursions in $\mathcal{T}_{11}(x_1)$ changes, this behavior does not mean that we get good predictions for $\tau_{11}(x_1)$. Quite interestingly, the degree of stress "intermittency" appears to be captured much better by the Smagorinsky and SGS energy models than by the constant eddy-viscosity model. The first two models depend locally on squared velocity differences, which are more intermittent than their first power. Nevertheless, according to Sec. II, higher-order moments of the stresses themselves were not found to be directly relevant to the energy dynamics of the

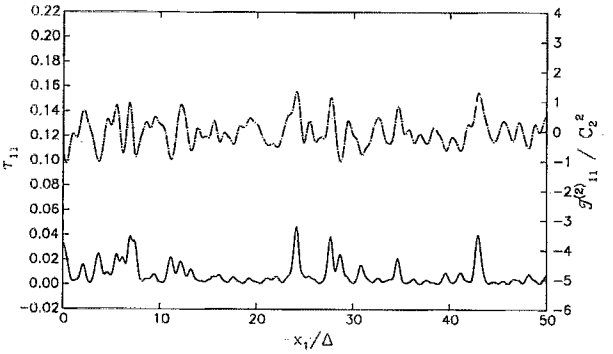

FIG. 7. Measured traces of the 11 element of the SGS stress tensor. ——: Real stress $\tau_{11}(x_1)$; - · -: modeled stress $\mathcal{T}_{11}^{(2)}(x_1)/C_2^2$ using the constant eddy-viscosity model (without the model constant). Gaussian filter with $\Delta = 32\eta$.

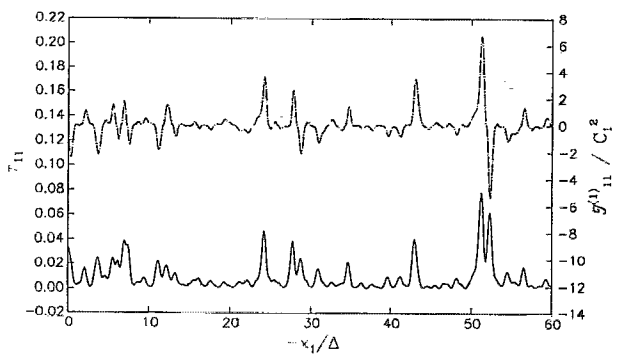

FIG. 6. Measured traces of the 11 element of the SGS stress tensor. ——: Real stress $\tau_{11}(x_1)$; - · -: modeled stress $\mathcal{T}_{11}^{(1)}(x_1)/C_1^2$ using the Smagorinsky model (without the model constant). Gaussian filter with $\Delta = 32\eta$.

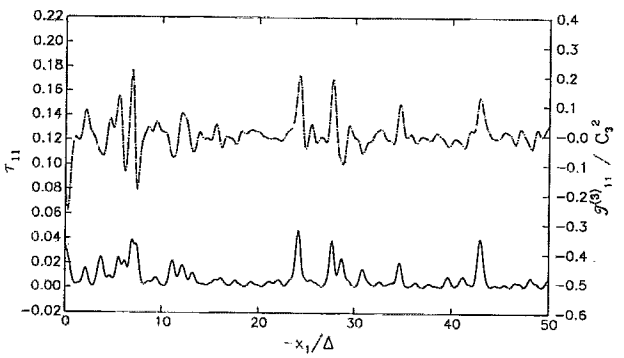

FIG. 8. Measured traces of the 11 element of the SGS stress tensor. ——: Real stress $\tau_{11}(x_1)$; - · -: modeled stress $\mathcal{T}_{11}^{(3)}(x_1)/C_3^2$ using the SGS kinetic energy model (without the model constant). Gaussian filter with $\Delta = 37\eta$.

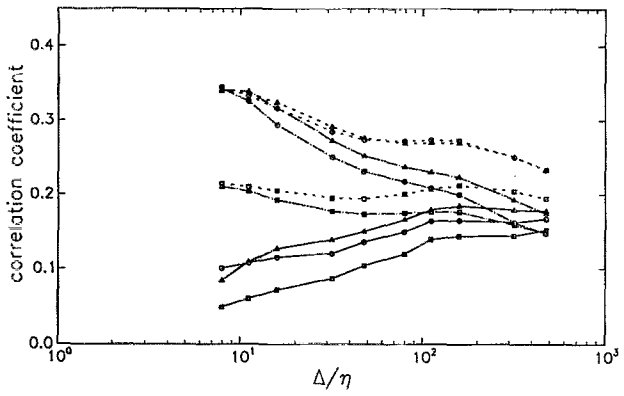

FIG. 9. Measured correlation coefficient between real and modeled SGS stress tensors, τ_{11} and $\mathscr{T}_{11}^{(i)}$. ——: Cutoff filtering, ···: Gaussian filtering; -·-: top-hat filtering. Circles: Smagorinsky model; squares: constant eddy viscosity; triangles: kinetic energy.

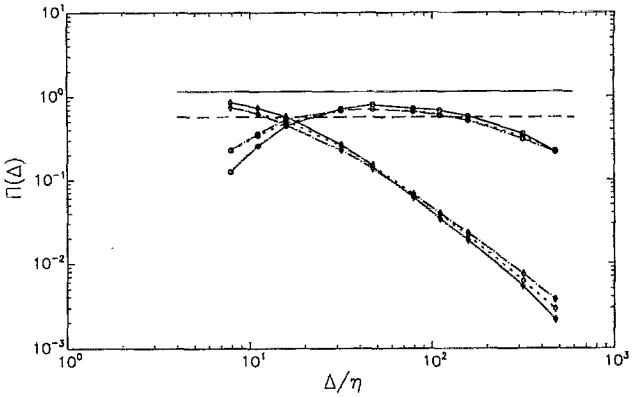

FIG. 10. Measured energy fluxes as function of filter width. Circles: SGS flux $\Pi_\Delta = -\frac{15}{2}\langle\tau_{11}\tilde{S}_{11}\rangle$. Diamonds: viscous dissipation rate ϵ_Δ. ——: cutoff filter, ···: Gaussian; -·-: top hat. Upper horizontal line: molecular dissipation $\langle\epsilon\rangle$; lower horizontal line: large-scale estimate $u_1'^3/L_1$.

resolved field. Therefore, we continue the analysis of the constant eddy viscosity model as well.

Results on other models, such as Bardina's similarity model, etc., will be reported elsewhere.[17,24]

C. General results

1. Correlation with models

To quantify previous observations, the correlation coefficient between τ_{11} and $\mathscr{T}_{11}^{(i)}$ is computed, for the three filter types considered. Figure 9 shows that this correlation is very low, for the entire range of relevant values of Δ, filter types, and models considered. This is quite consistent with the low degree of correlation that has been noted before in *a priori* testing from DNS databases [e.g., in Clark *et al.* (1979),[9] McMillan and Ferziger (1979),[10] Piomelli (1988),[11] Meneveau *et al.* (1992),[12] etc.]. However, the correlation ρ between the absolute values $|\tau_{11}|$ and $|\mathscr{T}_{11}^{(i)}|$ is much higher. For example, for the cutoff filter at $\Delta=32\eta$, one obtains $\rho=0.47$, 0.40, and 0.52 for the Smagorinsky, constant ν_T and kinetic energy models, respectively, while the values are $\rho=0.88$, 0.8, and 0.92 for the Gaussian filter. This result does not appear to have immediate utility besides showing that "activity" in the strain rate is accompanied by high SGS stress values.

2. Subgrid and viscous fluxes of kinetic energy

Several forms of energy flux to smaller scales are now compared. (a) The rate of dissipation $\langle\epsilon\rangle$ computed as in Eq. (56); (b) the large-scale estimate $u_1'^3/L_1$; and (c) the energy drain on the resolved motion at scale Δ:

$$\Pi_\Delta = -\tfrac{15}{2}\langle\tau_{11}\tilde{S}_{11}\rangle; \tag{71}$$

(d) The viscous dissipation of kinetic energy at scale Δ is also of interest:

$$\epsilon_\Delta = 15\nu\langle\tilde{S}_{11}^2\rangle. \tag{72}$$

The inertial range scaling of this quantity is

$$\epsilon_\Delta \sim \nu\langle\epsilon\rangle^{2/3}\Delta^{-4/3}. \tag{73}$$

These fluxes are computed as a function of Δ, for the different filter types, and they are shown in Fig. 10. The dissipation $\langle\epsilon\rangle$ and the large-scale estimate $u_1'^3/L_1$ are displayed for comparison. The trends observed are as expected: Π_Δ displays a plateau of the same order of magnitude as $\langle\epsilon\rangle$ or of u'^3/L_1. The decay of ϵ_Δ also follows the expected trend. Interestingly, Π_Δ and ϵ_Δ are of the same magnitude at about $\Delta/\eta\sim 20$, usually argued to be about the lower limit of the inertial range. Above $\Delta\sim 50\eta$ (say), the viscous flux becomes very small, less than 15% of the SGS flux.

D. Model constants

1. Model constants from measured energy balance

The model constants can be obtained, based on the condition that both the modeled and the real SGS energy flux must be the same:

(a) Smagorinsky: $$C_1^2 = \frac{\langle\tilde{S}_{11}\tau_{11}\rangle}{-2\Delta^2\langle\sqrt{15\tilde{S}_{11}^2}\tilde{S}_{11}^2\rangle}; \tag{74}$$

(b) constant eddy viscosity:

$$C_2^2 = \frac{\langle\tilde{S}_{11}\tau_{11}\rangle}{-2\Delta^2\sqrt{15\langle\tilde{S}_{11}^2\rangle}\langle\tilde{S}_{11}^2\rangle}; \tag{75}$$

and

(c) SGS kinetic energy: $$C_3^2 = \frac{\langle\tilde{S}_{11}\tau_{11}\rangle}{-2\Delta\langle\sqrt{|q^2|}\tilde{S}_{11}^2\rangle}. \tag{76}$$

Plots of C_i as a function of filter width Δ are provided in Figs. 11–13 for the three filter types. To a first approximation these values are fairly constant over the range of Δ values of interest. For the Smagorinsky model and constant eddy viscosity there is some difference between the cutoff filter results, which increase slowly with Δ, and the other two, which are considerably less dependent on Δ. The trend is reversed for the SGS kinetic energy model constant. Nevertheless, the *structure* of the eddy-viscosity

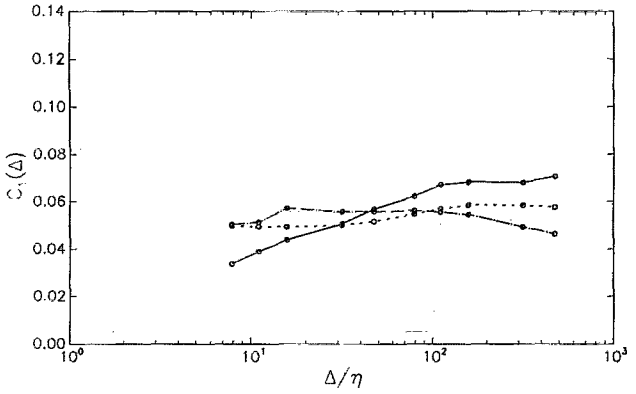

FIG. 11. Measured model constant for the Smagorsinsky eddy-viscosity model, as a function of filter width. ——: cutoff filter, ····: Gaussian; - · -: top hat.

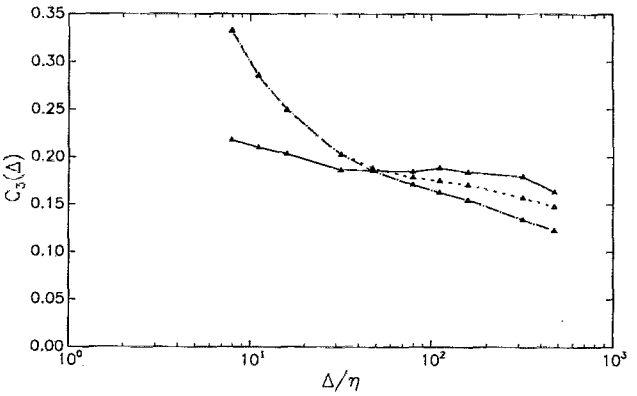

FIG. 13. Measured model constant for the SGS kinetic energy model, as a function of filter width. The captions are the same as in Fig. 11.

models appears to adequately reproduce the trends in energy flux with a constant C_i, independent of Δ, over the range of scales of interest. While Π_Δ in Fig. 10 varies by more than a factor of 5 between $\Delta=10\eta$ and 50η, the model constants change by less than 40% in the worst case (cutoff filter) in that same range.

Now we comment on the numerical value of the measured constants. Based on experience with LES and on a simple derivation assuming that Δ pertains to the inertial range,[31] the Smagorinsky constant C_s is usually chosen somewhere between 0.1 and 0.2 (for grid turbulence closer to 0.16, actually). Present results are considerably lower than those values. This discrepancy is possibly due to the one-dimensional filtering that is employed here. It causes the variance of $\tilde{S}_{11}$ to be overpredicted, since lateral fluctuations are not filtered out. To the degree that the correlation $\langle\tau_{11}\tilde{S}_{11}\rangle$ is not strongly affected, one obtains a lower value for the model constants. In the Appendix it is shown, using inertial range arguments, that the constant is indeed expected to be underpredicted by a factor of about 2 when one-dimensional instead of three-dimensional filtering is employed. From Fig. 11 one obtains a representative value of about $C_1\sim0.055$. When multiplied by the correction factor for one-dimensional averaging (see the Appendix), one obtains $C_s\sim0.11$, which is closer to the range of values usually employed.

From this discussion it is apparent that great care has to be taken in the interpretation of precise numerical values deduced from present experimental tests. For this reason we shall be interested more in observing qualitative trends, which are representative of the structure of a model.

2. Model constants from measured enstrophy dissipation

Instead of obtaining the model constants based on balance of energy, we can instead employ Eq. (49) and require that both real and modeled stresses generate the same SGS dissipation of enstrophy:

(a) Smagorinsky:
$$C_1^2=\frac{\langle(\partial^3\tilde{u}_1/\partial x_1^3)\tau_{11}\rangle}{-2\Delta^2\langle(\partial^3\tilde{u}_1/\partial x_1^3)\sqrt{15\tilde{S}_{11}^2}\tilde{S}_{11}\rangle}; \tag{77}$$

(b) constant eddy viscosity:
$$C_2^2=\frac{\langle(\partial^3\tilde{u}_1/\partial x_1^3)\tau_{11}\rangle}{-2\Delta^2\sqrt{15\langle\tilde{S}_{11}^2\rangle}\langle(\partial^3\tilde{u}_1/\partial x_1^3)\tilde{S}_{11}\rangle}; \tag{78}$$

and

(c) SGS kinetic energy:
$$C_3^2=\frac{\langle(\partial^3\tilde{u}_1/\partial x_1^3)\tau_{11}\rangle}{-2\Delta\langle(\partial^3\tilde{u}_1/\partial x_1^3)\sqrt{|\tilde{q}^2|}\tilde{S}_{11}\rangle}. \tag{79}$$

In order to avoid some very high-frequency corruption when taking the third-order derivatives of $\tilde{u}_1$, this variable is filtered after each differentiation with a Gaussian filter of (small) width $\Delta/10$. This procedure has practically no effect on the statistics computed, for the cutoff and Gaussian filter. It is done anyway because a trace of $\partial^3\tilde{u}_1/\partial x_1^3$ vs x_1 without this additional smoothing at scales much smaller than Δ has a very "noisy" appearance. For the top-hat filter there are indeed some differences when taking the required higher-order derivatives with or without the smoothing; therefore no results are presented for this case.

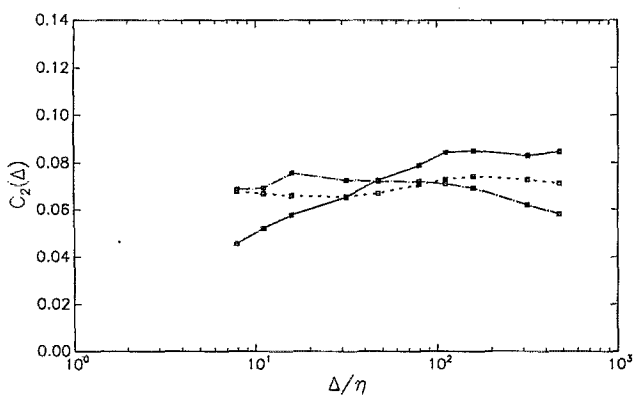

FIG. 12. Measured model constant for the constant eddy viscosity model, as a function of filter width. The captions are the same as in Fig. 11.

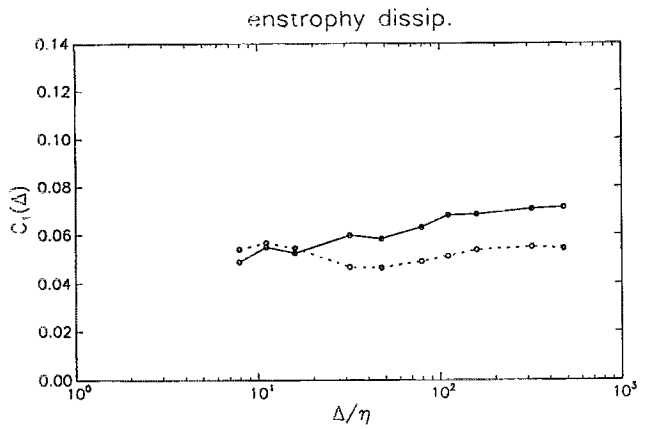

FIG. 14. Measured model constant for the Smagorsinsky eddy-viscosity model, enforcing the correct enstrophy dissipation. ——: cutoff, ···: Gaussian.

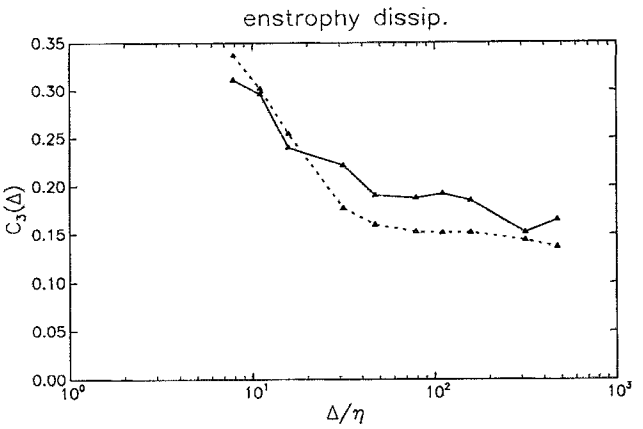

FIG. 16. Measured model constant for the SGS kinetic energy model, enforcing the correct enstrophy dissipation. ——: cutoff, ···: Gaussian.

The calculations are repeated for different values of Δ, and the results are presented in Figs. 14–16, for the cutoff and Gaussian filters. We observe that for $\Delta/\eta > 30$ (i.e., in the inertial range) the constants so computed are quite consistent with those arising from the balance of energy dissipation. Thus one could argue that, according to the discussion in Sec. II D 2, a LES with these models will produce the correct value for the third-order moments of velocity derivatives, in isotropic turbulence. For lower values of Δ, the constants required are larger than those required for energy balance. If one uses the constants obtained from the energy-flux balance, the modeled rates of enstrophy dissipation would be smaller than the measured SGS values. During a LES (with $\Delta < 30\eta$) this could result in a pileup of enstrophy at wave numbers close to the cutoff. However, one must remember that this discussion is based on the assumption that 1-D filtering produces trends comparable to 3-D filtering.

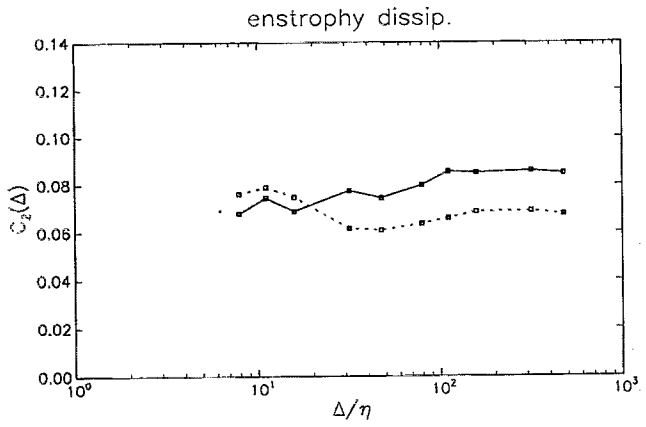

FIG. 15. Measured model constant for the constant eddy-viscosity model, enforcing the correct enstrophy dissipation. ——: cutoff, ···: Gaussian.

3. Model constants from resolved enstrophy balance

Continuing with the balance of enstrophy, we notice that the condition in Eq. (48) could also be used to evaluate the model constants by requiring that

$$\left\langle \left(\frac{\partial \tilde{u}_1}{\partial x_1}\right)^3 \right\rangle = -\left\langle \frac{\partial^3 \tilde{u}_1}{\partial x_1^3} \mathcal{T}_{11} \right\rangle. \tag{80}$$

The interesting feature of this relation is that it involves only statistics of resolved features of the flow. The fundamental difference with the balance of energy flux is that the production of enstrophy [represented here by the LHS of Eq. (80)] also occurs near the smallest resolved scales. Therefore, the model constants can be computed as

(a) Smagorinsky:
$$C_1^2 = \frac{\langle (\partial \tilde{u}_1/\partial x_1)^3 \rangle}{-2\Delta^2 \langle (\partial^3 \tilde{u}_1/\partial x_1^3) \sqrt{15 \tilde{S}_{11}^2} \tilde{S}_{11} \rangle}; \tag{81}$$

(b) constant eddy viscosity:

$$C_2^2 = \frac{\langle (\partial \tilde{u}_1/\partial x_1)^3 \rangle}{-2\Delta^2 \sqrt{15 \langle \tilde{S}_{11}^2 \rangle} \langle (\partial^3 \tilde{u}_1/\partial x_1^3) \tilde{S}_{11} \rangle}; \tag{82}$$

and

(c) SGS kinetic energy:

$$C_3^2 = \frac{\langle (\partial \tilde{u}_1/\partial x_1)^3 \rangle}{-2\Delta \langle (\partial^3 \tilde{u}_1/\partial x_1^3) \sqrt{|\tilde{q}^2|} \tilde{S}_{11} \rangle}. \tag{83}$$

The results are shown in Figs. 17–19. Again, there is good agreement with the values obtained before, except for the kinetic energy model for which the model constant continues to decrease even above $\Delta/\eta = 30$.

4. A new model based on enstrophy balance

The fact that one can obtain the model constants from the resolved fields suggests the possibility of a new model based on enstrophy equilibrium. Using Eq. (52) without

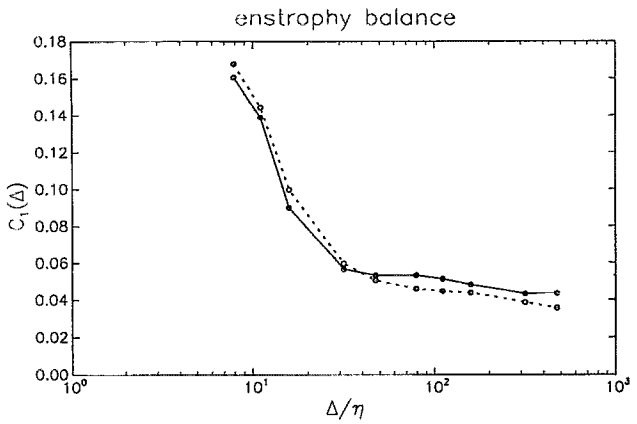

FIG. 17. Measured model constant for the Smagorsinsky eddy viscosity model, enforcing balance of enstrophy production and dissipation. ——: cutoff filter, ···: Gaussian.

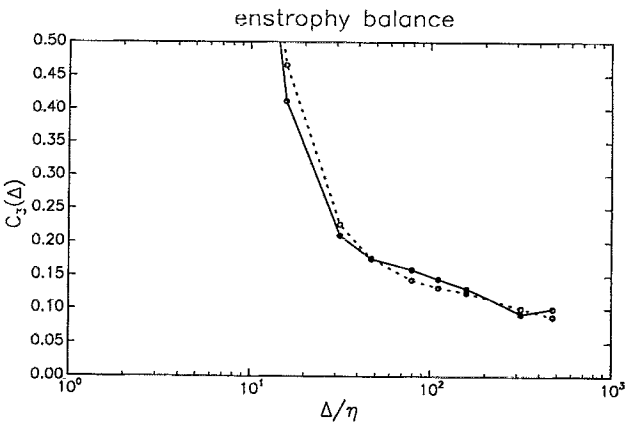

FIG. 19. Measured model constant for the SGS kinetic energy model, enforcing balance of enstrophy production and dissipation. ——: cutoff, ···: Gaussian.

the averaging, and computing a "local" value for (say) the Smagorinsky constant, one obtains the following "enstrophy" model:

$$\nu_T=\frac{\tilde{\omega}_p\tilde{\omega}_q\tilde{S}_{pq}}{4(\sqrt{2\tilde{S}_{mn}\tilde{S}_{mn}}\tilde{S}_{lj})(\partial^2\tilde{R}_{jk}/\partial x_k\,\partial x_l)}\sqrt{2\tilde{S}_{pq}\tilde{S}_{pq}},$$

where

$$\tilde{R}_{ij}=-\frac{1}{2}\epsilon_{ijk}\tilde{\omega}_k. \tag{84}$$

When Δ approaches the Kolmogorov scale, one should also subtract the enstrophy dissipation caused by molecular viscosity, $\nu(\nabla\tilde{\omega})^2$, from the numerator. This, in fact, is the reason for the high values at low Δ in Figs. 17–19. Relation (84) can be interpreted by saying that the enstrophy balance is used to obtain the appropriate length scale of the model. An interesting feature of this expression for ν_T is that it vanishes in irrotational flow (since the numerator contains a higher power of vorticity than the denominator). Also, it does not contain any free parameter, not even the width of the test filter that must be prescribed in the "dynamic model" of Germano *et al.*[3] However, it suffers from a difficulty similar to the "dynamic model" in its original formulation:[3] the denominator has zero crossings. This difficulty can be remedied to some degree by averaging over homogeneous directions, if they exist, or by time averaging:

$$\nu_T=\frac{\langle\tilde{\omega}_p\tilde{\omega}_q\tilde{S}_{pq}\rangle}{4\langle\sqrt{2\tilde{S}_{mn}\tilde{S}_{mn}}\tilde{S}_{lj}(\partial^2\tilde{R}_{jk}/\partial x_k\,\partial x_l)\rangle}\sqrt{2\tilde{S}_{pq}\tilde{S}_{pq}}. \tag{85}$$

Nevertheless, additional problems can be expected in its implementation since it is not clear how an actual LES would "adjust" to such a model. Because the constant is computed through an expression that is obtained directly from the N–S equations the following scenario is possible: Assume that one chooses an initial value for C_s and performs the LES in order to evaluate the average production and modeled SGS dissipation. It is possible that the LES will "adjust" so that the production and SGS dissipation of enstrophy are balanced no matter what constant was used as an initial guess. When evaluating it according to Eq. (87), one would thus obtain the same value assumed as the initial guess. Finally, the need to evaluate higher-order derivatives can cause additional problems. Without *a posteriori* testing, it is therefore not possible to further ascertain the merits of such an enstrophy model.

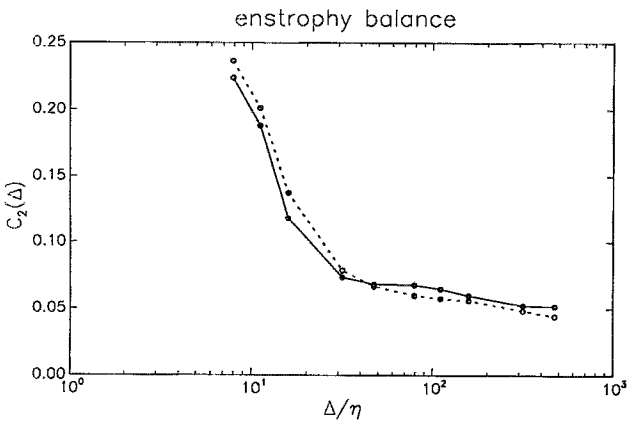

FIG. 18. Measured model constant for the constant eddy-viscosity model, enforcing balance of enstrophy production and dissipation. ——: cutoff filter, ···: Gaussian.

E. The velocity–stress correlation function

1. SGS stress correlation

In this section the velocity–stress correlation function is measured. After obtaining the filtered velocity and the stress, the two-point correlation functions,

$$G_\Delta(r)=\langle\tilde{u}_1(x_1+r)\tau_{11}(x_1)\rangle, \tag{86}$$

are computed using FFTs. Results for the cutoff filter using different values of Δ are shown in Fig. 20. The correlation functions are normalized based on the large-scale estimate

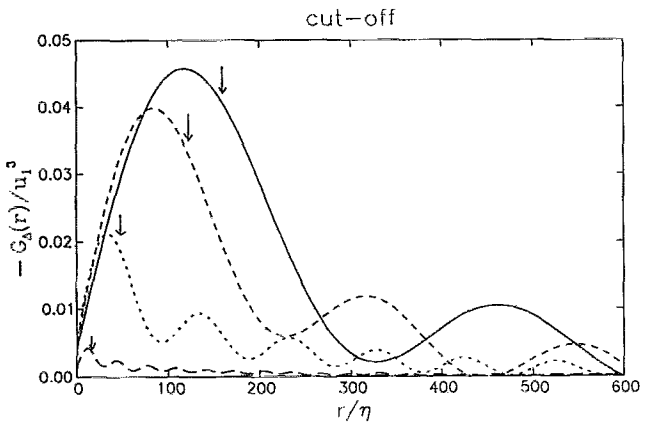

FIG. 20. Velocity–stress correlation function measured in grid turbulence using the cutoff filter. ——: $\Delta=160\eta$, ---: $\Delta=122\eta$, ···: $\Delta=48\eta$; and —·—: $\Delta=16\eta$.

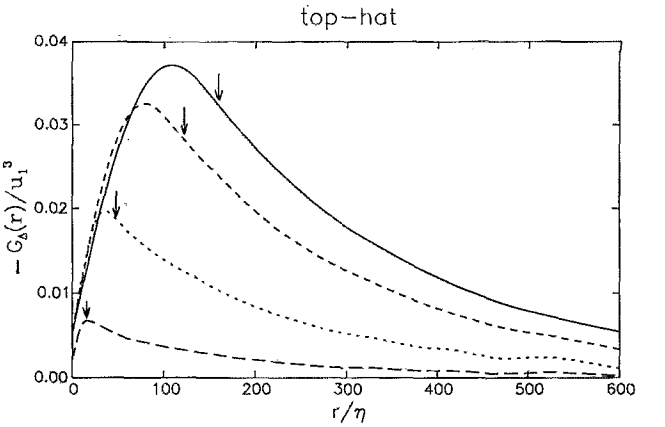

FIG. 22. Velocity–stress correlation function measured in grid turbulence using the top-hat filter, for different filter widths. The legend is as in Fig. 20.

$\langle\epsilon\rangle$ L_1, while r is normalized with η. The corresponding Δ values are indicated with the arrows. Similar results for Gaussian and top-hat filtering are shown in Figs. 21 and 22. The general shape of these curves is indeed as expected from the discussion in Sec. II D 2. The slope at the origin, equal to $\langle\tilde{S}_{11}\tau_{11}\rangle$, is seen to be almost independent of Δ, which is consistent with the constancy of the energy flux. It can also be observed that $G_\Delta(r)$ does not exactly vanish at $r=0$ as it should in isotropic turbulence. We recall that since even the velocity skewness is not exactly zero, small deviations from isotropy are to be expected.

For the cutoff filter, oscillations can be observed. They are due to the "lobes" of the filter. When $r=r_n=(4n+1)\Delta/2$ the filter has local peaks, meaning that $\tilde{u}_1(x+r_n)$ will contain some contribution from the velocity at x. Since the velocity there makes a direct contribution to $\tau_{11}(x)$, one obtains an increase in the correlation between $\tilde{u}_1(x+r)$ and $\tau_{11}(x)$ when $r=r_n$. On the other hand, no significant differences are observed between the results corresponding to the Gaussian and top-hat filters.

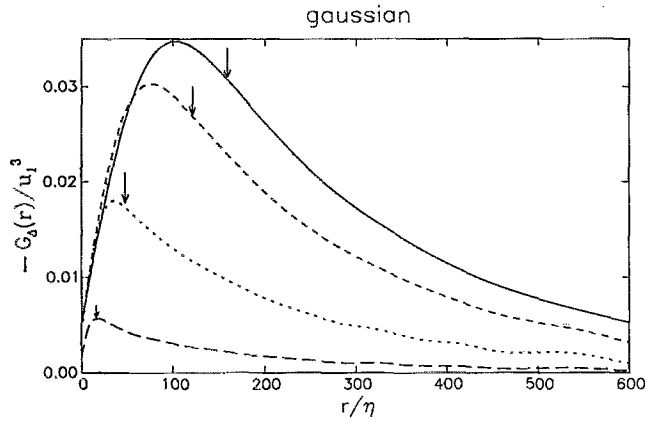

FIG. 21. Velocity–stress correlation function measured in grid turbulence using the Gaussian filter, for different filter widths. The legend is as in Fig. 20.

The plots suggest the possibility of scaling with Δ. This is shown in Fig. 23 for the Gaussian filter. Although the curves peak at similar values of r/Δ, the curves do not collapse. This observation implies that a "universal" SGS dissipation spectrum (in which Δ takes on the role of the Kolmogorov scale) does not exist for this flow. This is not surprising given the moderate Reynolds number. We now elaborate a little further on the notion of a SGS dissipation spectrum. Starting from Eq. (40) it is easy to show that (in isotropic turbulence) $\tilde{E}(k,t)$, the three-dimensional radial spectrum of the resolved field, obeys

$$\left(\frac{\partial}{\partial t}-2\nu k^2\right)\tilde{E}(k,t)-\tilde{T}(k,t)=H(k,t). \tag{87}$$

Here

$$H(k,t)=\frac{k}{\pi}\int_0^\infty G_{LLL}(r,t)[3\sin(kr)-3kr\cos(kr) -k^2r^2\sin(kr)]dr, \tag{88}$$

is the "SGS dissipation spectrum." We remark that it can be used to define a wave-number-dependent eddy viscosity.[32] The transfer spectrum $\tilde{T}(k,t)$ consists of triple products of resolved velocities, and does not occupy our interest here. To the degree that present measurements of $G_\Delta(r)=\langle\tilde{u}_1(x+r)\tau_{11}(x)\rangle$ are representative of $G_{LLL}(r)$ (keep in mind the 1-D averaging, lack of exact isotropy, etc.) self-similarity of $G_{LLL}(r)$ would have implied that $H(k)$ could also be rescaled:

$$h(\xi)=\frac{H(k)}{\langle\epsilon\rangle\Delta},\quad \xi=k\Delta. \tag{89}$$

It is possible that such a collapse may occur at higher Reynolds numbers. We have attempted to compute $H(k)$ according to Eq. (88) using the measured correlation function $G_\Delta(r)$ instead of $G_{LLL}(r,t)$. However, small oscillations in $G_\Delta(r)$ and deviations from isotropy are enough to render the integral very unstable. Large and unphysical

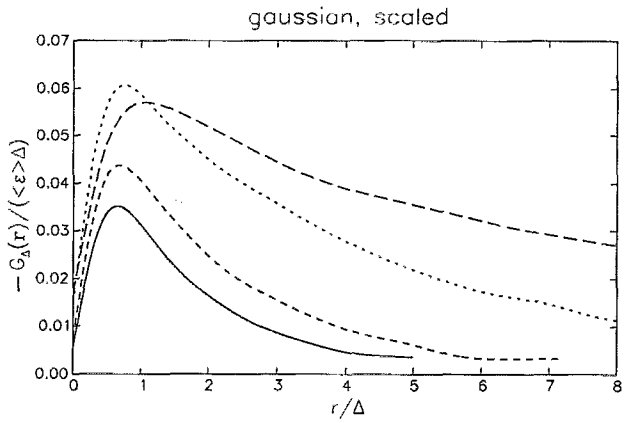

FIG. 23. Scaled velocity–stress correlation function measured using the Gaussian filter. The legend is as in Fig. 20.

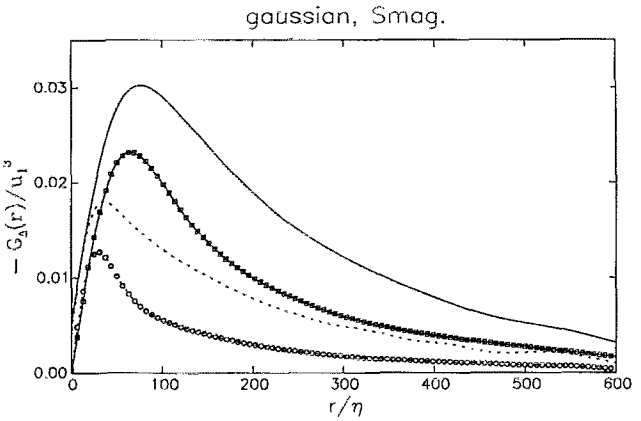

FIG. 25. Real and modeled velocity–stress correlation function, using the Gaussian filter, and the Smagorinsky model. The legend is the same as in Fig. 24.

oscillations in $H(k)$ resulted from this procedure and we therefore have to refrain from transforming our experimental results to (radial) Fourier space.

Next, we recall that a good SGS model should reproduce the measured correlation functions as a necessary condition for LES to generate the correct energy spectrum. This is explored in the next sections.

2. Modeled velocity–stress correlation function

We have already established that the data supports an approximately constant value for the model constants (see Figs. 11, etc.). The purpose of this section is to test whether the models also correctly reproduce the two-point structure observed in the previous section. In order to separate this issue from the precise value of the model constant, the latter is selected such that the correct energy flux is guaranteed, at every Δ. In other words, the model constant is chosen at each Δ according to Eq. (74). Then the modeled correlation function $\langle \tilde{u}_1(x+r)\mathcal{T}_{11}(x)\rangle$ is computed. The results corresponding to the Smagorinsky model are presented in Figs. 24–26 for the different filter types. Two representative values, $\Delta=48\eta$ and $\Delta=122\eta$, are presented; results for other Δ values follow essentially the same trends. Results for the constant eddy viscosity and SGS kinetic energy models are presented using the Gaussian filter in Figs. 27 and 28.

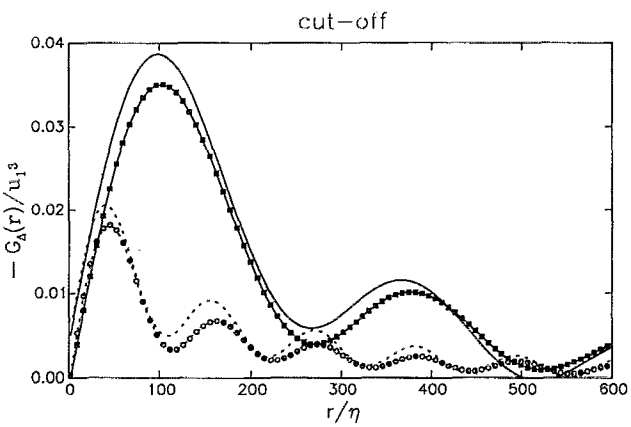

FIG. 24. Real (lines) and modeled (symbols+lines) velocity–stress correlation function, using the cutoff filter, and the Smagorinsky model. Solid lines: $\Delta=122\eta$; dotted lines: $\Delta=48\eta$.

The main observation is that the trends are well modeled by the various eddy-viscosity models: Both modeled and real correlation functions peak at about the same value of r, and then decay monotonically at a similar rate. For the cutoff filter and the top-hat filter at larger Δ values, the agreement is quite good. The difference is that for the Gaussian filter the modeled results fall below the real curve by about a factor of 2. This could, according to Eq. (47), generate a slight overprediction of the third-order structure functions from the LES. However, as one moves to $r \gg \Delta$, this becomes negligible. This is consistent with the commonly held view that two-point statistics at large distances $r \gg \Delta$ (or spectra at $k \ll \pi/\Delta$) will be largely unaffected by the details of the SGS model. Even for the Gaussian filter, the trends and type of decay agree quite well. This point is made clearer in Fig. 29, which is the same as Fig. 25 in log–log units. In addition, it is remarkable that (once scaled to have equal slope at the origin), there exists almost no difference between the predicted correlation functions from the three eddy-viscosity models.

We conclude that, to within the accuracy of present measurements, the statistics of the eddy-viscosity models are not inconsistent with those of the real SGS stresses. Therefore, the models comply reasonably well with the necessary conditions (in terms of trends) to accurately reproduce the two-point statistics or the energy spectrum of the resolved velocity, in grid turbulence.

IV. SUMMARY AND CONCLUSIONS

Statistical features of subgrid-scale models for Large-Eddy Simulations were considered. In the first part of this paper, necessary conditions that they should obey in order to "cause" the correct resolved fields in a LES were derived. The "turbulence problem" of the resolved velocity

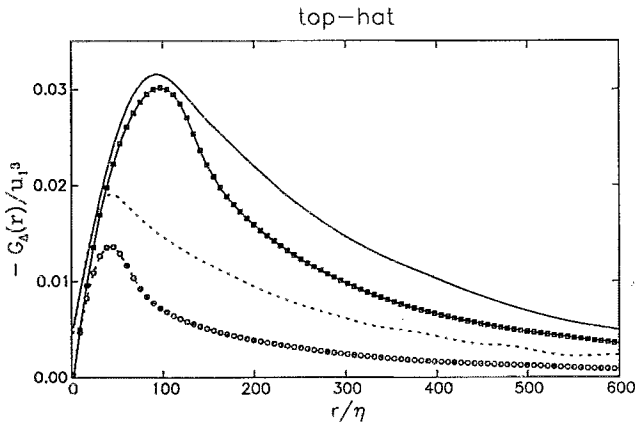

FIG. 26. Real and modeled velocity–stress correlation function, using the top-hat filter for the Smagorisnsky model. The same legend as in Fig. 24.

field was shown to severely weaken our ability to establish sufficient conditions. At any order, an equation for, say, $A^{(n)}$ (a resolved moment of order n) could be employed to state conditions on the SGS stresses. But these were necessary to enable the correct prediction of *both* $A^{(n)}$ and $A^{(n+1)}$ (in addition to a moment involving the model expression). If, however, one did not care about $A^{(n+1)}$ but only about $A^{(n)}$, no way of separating the effect of errors in the model between $A^{(n)}$ and $A^{(n+1)}$ was found. Nevertheless, it was argued that necessary conditions can be a valuable tool to compare the properties of models through statistical *a priori* testing. A special case, where sufficient conditions could be obtained, was when third-order structure functions in locally isotropic turbulence were considered.

These basic considerations were illustrated with statistical *a priori* testing of three simple eddy-viscosity models, using experimental data in grid turbulence. Several major assumptions were made during the analysis, mainly because of limitations in the data available. Each of them was sufficiently strong to make a quantitative interpretation of the results very difficult, although qualitative trends were argued to be robust and were used to make several new observations. The main assumptions were: (a) That filtering along a single direction would give results similar to three-dimensional filtering. It was shown analytically that this assumption cannot strictly be true, since it can have an effect on the numerical value of the model constants. Also, the resulting large-scale field ceases to be isotropic and therefore a dynamical equation at a scalar level [such as Eq. (40)] cannot hold exactly. Nevertheless, the overall consistency between the flux $\frac{15}{2}\langle \tilde{S}_{11}\tau_{11}\rangle$ obtained from 1-D filtering and $\langle\epsilon\rangle$, for which no filtering is performed, lends some justification to assumption (a). We also presented an alternative interpretations of the results in terms of two-point statistics with anisotropic filtering (see the Appendix), which did not require us to make the isotropy assumption. (b) When computing the local eddy viscosities, instantaneous iso-tropy was assumed. This assumption was unnecessary in the case of the constant eddy-viscosity model. Although difficult to quantify, we do not believe that this assumption has a significant impact on the resulting statistics. (c) We did not subtract the trace of the measured SGS stress tensor. This was shown to be of no consequence in isotropic fields. Nevertheless, to the degree that the filtered fields are not isotropic, this can introduce additional errors. The combination of these assumptions clearly implies that any numerical values from the measurements have to be interpreted with great caution.

In terms of *trends*, the following results were obtained: (a) In agreement with previous experience in *a priori* testing, the real and modeled stresses exhibited almost no correlation at a local level. (b) All three eddy-viscosity models were shown to approximately reproduce the correct SGS energy dissipation with a model constant nearly independent of the filter width Δ. Fluctuations in eddy viscosity did not appear to have much impact, given the agreement with the constant eddy-viscosity model. Also, this insensitivity to eddy-viscosity fluctuations lends some qualified support to our hypothesis that the results are insensi-

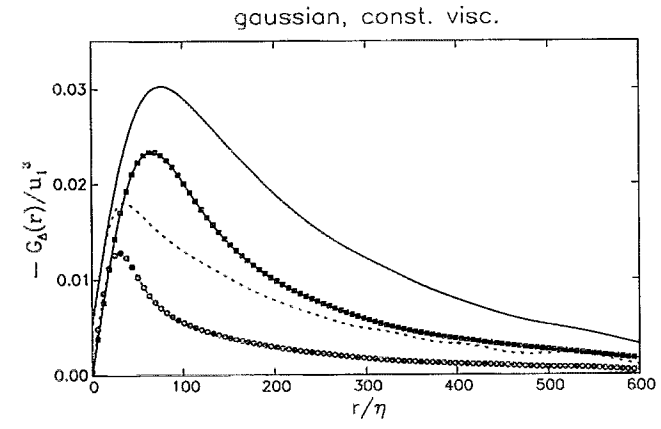

FIG. 27. Real and modeled velocity–stress correlation function, using the Gaussian filter for the constant eddy-viscosity model. The legend is the same as in Fig. 24.

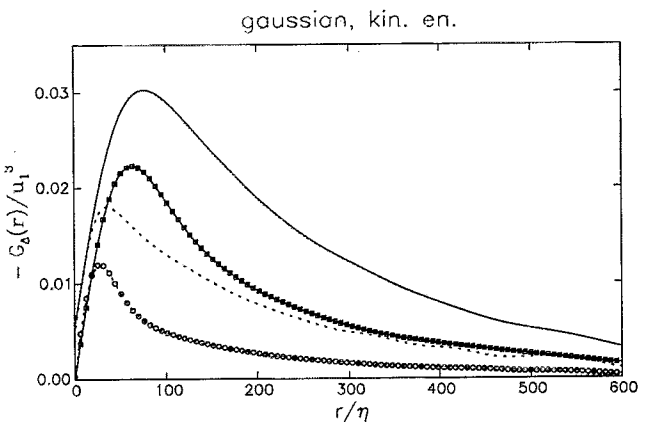

FIG. 28. Real and modeled velocity–stress correlation function, using the Gaussian filter for the kinetic energy model. The legend is the same as in Fig. 24.

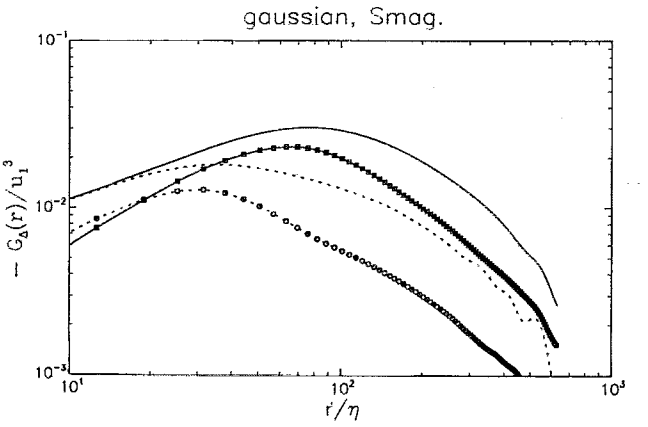

FIG. 29. Log–log plot of real (lines) and modeled (symbols+lines) velocity–stress correlation functions, using the Gaussian filter, and the Smagorinsky model. The legend is the same as in Fig. 24.

tive to evaluating the eddy viscosity based on one component rather than based on the true invariants. (c) The three eddy-viscosity models also reproduced the correct dissipation of enstrophy, within a significant range of Δ values. Using the fact that the production of enstrophy also occurs near the cutoff scale, some possibilities and risks for a new model based on enstrophy equilibrium were outlined. (d) The two-point correlation function between filtered velocity and SGS stress was shown to be adequately reproduced by the eddy-viscosity models. There was a discrepancy by a factor of about 2 for some cases, but given the assumptions reviewed above, we refrain from ascribing too much significance to this difference. The main result is that the trends are followed quite well. According to the discussion in Sec. II D, and under the assumptions already stated, the present results give an experimental justification to what has already been known from extensive experience with LES: Eddy-viscosity SGS closures contain the appropriate physics to enable them to generate acceptable energy spectra of the resolved portion of a LES flow field (of isotropic turbulence).

Clearly, with measurements of more velocity components in more dimensions,[17,24] the assumptions of this study can be narrowed considerably. Consequently, quantitative experimental results could then be interpreted in a stronger fashion. Also, tests in more complicated flows, involving other models, etc., is generating additional knowledge relevant to SGS modeling.

ACKNOWLEDGMENTS

The author thanks J. O'Neil for his assistance with the preprocessing of the grid turbulence data and with the measurements, T. Lund for thoughtful comments on the manuscript, and A. Scotti for comments on the Appendix. In addition, the author has benefited from discussions with J. Katz, O. Knio, P. Moin, G. Berkooz, M. Nelkin, P. Purtell, and S. Lekoudis. This work is supported by the National Science Foundation, Grant No. CTS-9113048 and the Office of Naval Research, Grant No. N00014-92-J-1109.

APPENDIX: IMPACT OF ONE-DIMENSIONAL FILTERING

In this appendix the influence of one-dimensional filtering on the numerical value of model constants is estimated. Following Lilly,[31] the rate of dissipation is calculated, assuming that the filter width pertains to the inertial range. Using an isotropic cutoff filter (denoted by an overcaret), and making the (relatively strong) assumption that $\langle \sqrt{\hat{S}_{mn}\hat{S}_{mn}}\hat{S}_{ij}\hat{S}_{ij}\rangle = \langle \hat{S}_{ij}\hat{S}_{ij}\rangle^{3/2}$, we can write

$$\langle \epsilon \rangle = -\langle \tau_{ij}\hat{S}_{ij}\rangle = (C_s\Delta)^2 15^{3/2}\left\langle \left(\frac{\partial \hat{u}_1}{\partial x_1}\right)^2 \right\rangle^{3/2}. \quad \text{(A1)}$$

Instead, if we use filtering in the x_1 direction only (denoted by an overtilde), and only consider the longitudinal component of the rate-of-strain tensor, we must use another constant C_1 according to

$$\langle \epsilon \rangle = (C_1\Delta)^2 15^{3/2}\left\langle \left(\frac{\partial \tilde{u}_1}{\partial x_1}\right)^2 \right\rangle^{3/2}. \quad \text{(A2)}$$

As in the main text, we continue to assume that $\tilde{\mathbf{u}}$ is an isotropic field (which is not strictly true). Now, if Δ pertains to the inertial range, we can evaluate the isotropically filtered gradient in terms of the 3-D radial spectrum

$$\left\langle \left(\frac{\partial \hat{u}_1}{\partial x_1}\right)^2 \right\rangle = \frac{2}{15}\int_0^{\pi/\Delta} C_k\langle\epsilon\rangle^{2/3}k^{1/3}\,dk = 0.46C_k\langle\epsilon\rangle^{2/3}\Delta^{-4/3}. \quad \text{(A3)}$$

The longitudinally filtered velocity gradient can be obtained as

$$\left\langle \left(\frac{\partial \tilde{u}_1}{\partial x_1}\right)^2 \right\rangle = \int_0^{\pi/\Delta} \frac{18}{55} C_k\langle\epsilon\rangle^{2/3}k_1^{1/3}\,dk_1 = 1.13C_k\langle\epsilon\rangle^{2/3}\Delta^{-4/3}. \quad \text{(A4)}$$

Therefore, the variance of the longitudinal velocity gradient filtered in only one direction is considerably higher than its counterpart involving the radial filter. (These arguments are generalized in Ref. 33.) If these results are replaced in Eqs. (A1) and (A2), one obtains

$$C_s = (15\cdot 0.46\cdot C_k)^{-3/4}, \quad \text{(A5)}$$

while

$$C_1 = (15\cdot 1.129\cdot C_k)^{-3/4}. \quad \text{(A6)}$$

Therefore $C_s \sim 1.96C_1$. This discussion illustrates the difficulty in using present experimental results to obtain numerical values for the model constants, which can be interpreted in the context of isotropic filtering. This circumstance is the reason that the attention in the main text is instead focused on general trends (such as scaling with Δ, r, etc.).

If, nevertheless, one wants to use the numerical values obtained in the experiments, one can make the argument that they should be relevant to LES with a highly noniso-

tropic grid. Consider a LES in which a coarse grid is used in the x_1 direction, while DNS is performed in the x_2 and x_3 directions. Let us now repeat Eq. (36), written for the 11 component, when the filtering is this 1-D filter in the x_1 direction:

$$\left(\frac{\partial}{\partial t}-2\nu\nabla_r^2\right)B_{11}(\mathbf{r}) = \frac{\partial}{\partial r_1}\frac{(\langle p\tilde{u}_1'\rangle-\langle p'\tilde{u}_1\rangle)}{\rho}+2\frac{\partial B_{1k,1}}{\partial r_k} +2\frac{\partial}{\partial r_k}\langle\tilde{u}_1(\mathbf{x}+\mathbf{r})\tau_{k1}(\mathbf{x})\rangle. \tag{A7}$$

A necessary condition to properly predict the last term on the RHS of this evolution equation is to obtain the correct value of the vector function $\langle\tilde{u}_1(\mathbf{x}+\mathbf{r})\tau_{k1}(\mathbf{x})\rangle$. For it to be properly modeled, each of its components (up to a divergence-free vector) must be correctly described by the SGS model, e.g., the component $\langle\tilde{u}_1(\mathbf{x}+\mathbf{r})\tau_{11}(\mathbf{x})\rangle$. The latter is a scalar function of a vector $\mathbf{r}$, assuming homogeneity with respect to $\mathbf{x}$. Our measurements of $\langle\tilde{u}_1(x+r_1)\tau_{11}(x)\rangle$ only deal with the values of this function along a single direction $\mathbf{r}=(r_1,0,0)$. However, if this last function is not correctly reproduced by a SGS closure, then we know that the vector function is not correctly predicted for *all* $\mathbf{r}$ values. Thus its divergence cannot be correct everywhere either (unless, with an arguably negligible probability, the divergence-free vector field that can be added exactly cancels the errors everywhere). Finally, one can argue that errors in $\langle\tilde{u}_1(x+r_1)\tau_{11}(x)\rangle$ will yield errors in the prediction of the rate of change of $B_{11}(\mathbf{r},t)$, the pressure–velocity correlation or the resolved third-order velocity moment $B_{1k,1}$. Thus

$$\langle\tilde{u}_1(x+r_1)\tau_{11}(x)\rangle=\langle\tilde{u}_1(x+r_1)\mathscr{T}_{11}(x)\rangle \tag{A8}$$

is a necessary condition for the correct evolution of the above-mentioned two-point correlation functions, even for nonisotropic filtering.

[1]W. C. Reynolds, "The potential and limitations of direct and large eddy simulations," in *Whither Turbulence? or Turbulence at Crossroads*, edited by J. L. Lumley (Springer, New York, 1990), p. 313.

[2]R. Rogallo and P. Moin, "Numerical simulation of turbulent flows," Annu. Rev. Fluid. Mech. **16**, 99 (1984).

[3]M. Germano, U. Piomelli, P. Moin, and W. H. Cabot, "A dynamic subgrid-scale eddy viscosity model," Phys. Fluids A **3**, 1760 (1991).

[4]D. K. Lilly, "A proposed modification of the Germano subgrid scale closure method," Phys. Fluids A **4**, 633 (1992).

[5]U. Piomelli, "High Reynolds number calculations using the dynamic subgrid-scale stress model," Phys. Fluids A **5**, 1484 (1993).

[6]K. Akselvoll and P. Moin, "Application of the dynamic localization model to large-eddy simulation of turbulent flow over a backward facing step," in *Engineering Applications of Large Eddy Simulations*, edited by U. Piomelli and S. Ragab (ASME, New York, 1993).

[7]L. Shtilman and J. R. Chasnov, "Les vs. dns: a comparative study," in *Proceedings of the Summer Program 1992 Stanford University*, 1992 (Center for Turbulence Research, Standord, CA, 1992), Vol. 3, p. 137.

[8]J. P. Boris, Comment 1. on "The potential and limitations of direct and large eddy simulations," in Ref. 1, p. 344.

[9]R. A. Clark, J. H. Ferziger, and W. C. Reynolds, "Evaluation of subgrid models using an accurately simulated turbulent flow," J. Fluid Mech. **91**, 1 (1979).

[10]O. J. McMillan and J. H. Ferziger, "Direct testing of subgrid-scale models," AIAA J. **17**, 1340 (1979).

[11]U. Piomelli, P. Moin, and J. H. Ferziger, "Model consistency in large eddy simulation of turbulent channel flows," Phys. Fluids **31**, 1884 (1988).

[12]C. Meneveau, T. Lund, and P. Moin, "Search for subgrid scale parametrization by projection pursuit regression," in Ref. 7, Vol. IV, p. 61.

[13]T. S. Lund and E. A. Novikov, "Parametrization of subgrid-scale stress by the velocity gradient tensor," in *Center for Turbulence Research, Annual Research Briefs* (Center for Turbulence Research, Stanford, CA, 1992), Vol. 27, p. 1992.

[14]J. A. Domaradski, W. Liu, and M. E. Brachet, "An analysis of subgrid-scale interactions in numerically simulated isotropic turbulence," Phys. Fluids A **5**, 1747 (1993).

[15]C. Härtel and L. Kleiser, "Energy transfer between large and small scales in wall-bounded turbulent flows," in *Engineering Applications of Large Eddy Simulations*, edited by U. Piomelli and S. Ragab (ASME, New York, 1993).

[16]K. Horiuti, "A proper velocity scale for modeling subgrid-scale eddy viscosities in large eddy simulation," Phys. Fluids A **5**, 146 (1993).

[17]S. Liu, C. Meneveau, and J. Katz, "On the properties of similarity subgrid-scale models as deduced from measurements in a turbulent jet," submitted for publication (1993).

[18]M. Germano, "Turbulence: the filtering approach," J. Fluid Mech. **238**, 325 (1992).

[19]T. S. Lundgren, "Distribution functions in the statistical theory of turbulence," Phys. Fluids, **10**, 969 (1967).

[20]S. B. Pope, "Pdf methods for turbulent reactive flows," Prog. Energy Combust. Sci. **11**, 119 (1985).

[21]G. Berkooz, "An observation on probability density equations, or, when do simulations reproduce statics," Preprint FDS-93-04, Cornell University (1993).

[22]A. Monin and A. Yaglom, *Statistical Fluid Mechanics* (MIT Press, Cambridge, MA, 1971).

[23]A. Leonard, "Energy cascade in large-eddy simulations of turbulent fluid flows," Adv. Geophys. **18**, 237 (1974).

[24]J. O'Neil and C. Meneveau, "Measurements of subgrid-scale stresses in the turbulent plane wake" (unpublished).

[25]G. Comte-Bellot and S. Corrsin, "The use of a contraction to improve the isotropy of grid generated turbulence," J. Fluid Mech. **66**, 657 (1966).

[26]J. O'Neil and C. Meneveau, "Spatial correlations in turbulence: Predictions from the multifractal formalism and comparison with experiments," Phys. Fluids A **5**, 158 (1993).

[27]S. V. Veeravalli and S. G. Saddoughi, "A preliminary experimental investigation of local isotropy in high-Reynolds-number turbulence," *Annual Research Briefs* (Center for Turbulence Research, Stanford, CA, 1991), pp. 3–20.

[28]P. Moin (private communication, 1992).

[29]V. C. Wong, "A proposed statistical-dynamic closure method for the linear of nonlinear subgrid-scale stresses," Phys. Fluids A **4**, 1081 (1992).

[30]S. Ghosal, T. S. Lund, and P. Moin, "A local dynamic model for large eddy simulation," in Ref. 13, Vol. 3.

[31]D. K. Lilly, "The representation of small-scale turbulence in numerical simulation experiments," in Proceedings of the IBM Scientific Computing Symposium on Environmental Sciences, 1967, p. 195.

[32]J.-P. Chollet and M. Lesieur, "Parametrization of small-scales of three-dimensional isotropic turbulence using spectral closures," J. Atmos. Sci. **38**, 2747 (1982).

[33]A. Scotti, C. Meneveau, and D. K. Lilly, "Generalized Smagorinsky model for anisotropic grids," Phys. Fluids A **5**, 2306 (1993).